GEOTECHNICAL ENGINEERING

MATERIALS STUDIES RELATED TO LUNAR SURFACE EXPLORATION

by

J. K. MITCHELL
I. S. E. CARMICHAEL
R. E. GOODMAN
J. FRISCH
P. A. WITHERSPOON
F. E. HEUZÉ

FINAL REPORT: VOLUME IV OF IV

PREPARED FOR MARSHALL SPACE FLIGHT CENTER
HUNTSVILLE, ALABAMA UNDER NASA CONTRACT
NSR 05-003-189

MARCH, 1969

SPACE SCIENCES LABORATORY

UNIVERSITY OF CALIFORNIA · BERKELEY

G E O T E C H N I C A L E N G I N E E R I N G

MATERIAL STUDIES RELATED TO LUNAR SURFACE EXPLORATION

By

James K. Mitchell
Ian C. Carmichael
Joseph Frisch
Richard E. Goodman
Paul A. Witherspoon
Francois E. Heuzé

FINAL REPORT: VOLUME IV OF IV

Prepared for Marshall Space Flight Center
Huntsville, Alabama, under NASA Contract
NSR 05-003-189

March 1969

Space Sciences Laboratory

University of California, Berkeley 94720

TABLE OF CONTENTS

LIST OF ILLUSTRATIONS

CHAPTER 1

CHAPTER 2

LIST OF TABLES

CHAPTER 1

PREFACE

This report presents in its four volumes the results of studies conducted during the period March 6, 1967 — June 30, 1968, under NASA research contract NSR 05-003-189, "Materials Studies Related to Lunar Surface Exploration." This study was sponsored by the Advanced Lunar Missions Directorate, NASA Headquarters, and was under the technical cognizance of Dr. N. C. Costes, Space Sciences Laboratory, George C. Marshall Space Flight Center.

This report reflects the combined effort of five faculty investigators and a full time project manager/engineer assisted by six graduate research assistants, representing several engineering and scientific disciplines pertinent to study of lunar surface material properties. James K. Mitchell, Professor of Civil Engineering, served as Principal Investigator and was responsible for those phases of the work concerned with problems relating to lunar soil mechanics and the engineering properties of lunar soils. Co-investigators were Ian C. Carmichael, Professor of Geology, in charge of geological studies; Joseph Frisch, Professor of Mechanical Engineering, who was responsible for analysis of friction and adhesion problems and the testing of materials under high-vacuum conditions; Richard E. Goodman, Associate Professor of Geological Engineering, who was concerned with the engineering geology and rock mechanics aspects of the lunar surface; and Paul A. Witherspoon, Professor of Geological Engineering, who conducted studies related to thermal and permeability measurements on the lunar surface. Francois E. Heuzé, Assistant Specialist, served as project manager and contributed to studies in the areas of rock mechanics and engineering geology.

INTRODUCTION

I. OBJECTIVES

It is axiomatic that, among the myriad of technical and scientific factors that must be considered in the lunar exploration program, the nature of lunar soil and rock surface materials is of prime importance in the design of spacecraft landing systems, the design of surface mobility systems, the design of experiments to be conducted on the lunar surface, mission planning, and, ultimately, to mission success. Without specific knowledge of the mechanical properties of lunar soils, designers and mission planners have no choice but to adopt ultraconservative designs and procedures in an effort to insure astronaut safety. Thus it is of paramount importance that as much specific information as possible about lunar surface material properties be obtained prior to the first manned lunar mission, and that planning and design options for further missions remain open thereafter in order to accommodate changes as more and more specific data become available.

The study described in this report was initiated in an effort to better define both the surface material related engineering problems and the relevant properties of the materials themselves. Information developed as a result of this effort was then utilized in specific studies of problems considered to be of critical importance and for the development of analysis and testing methods that appear particularly promising for the study of lunar surface properties by both remote and tactile means.

Specific objectives that were set at the onset of the study were:

1. To define geological and engineering problems associated with on-site lunar exploartion dependent on knowledge of soil and rock properties for solution.

2. To critically evaluate current knowledge concerning lunar surface materials, their properties, and their relationships to problems associated with on-site lunar exploration, and to select reasonable models for lunar surface conditions.

3. To make preliminary formulations of desirable on-site soil and rock mechanics studies for extended lunar exploration and to make recommendations as to appropriate apparatus and required astronaut skills for performance of such investigations.

4. To undertake preliminary studies for development of rock testing devices for use in a borehole on the lunar surface for the determination of the stress-strain characteristics of rocks.

5. To review friction and adhesion problems and to make recommendations for improved design of existing apparatus for determination of frictional and adhesive characteristics of different metallic and nonmetallic materials under high vacuum and at high and low temperatures.

6. To make recommendations and cost estimates for the design of apparatus for measuring silicate mineral solubility and viscosity at high temperatures and pressures and for determining the distribution of silicates between gas and liquid phases.

7. To review critically theories for the origin of the moon and to consider logical sequences for investigations to be carried out on the lunar surface for most efficient determination of composition, structure and history of the moon.

The results of studies of this type are intended to aid in attainment of the following longer range goals:

1. Development of capability for predicting, at least in a semi-quantitative manner, soil conditions at any point on the moon on the basis of remote measurements.

2. Development of capability for detailed quantitative determination of soil and rock properties at any chosen site where scientific or engineering work is contemplated.

3. Development of methods of analysis suitable for solution of soil and rock mechanics problems on the moon.

4. Utilization of the information obtained, both as an aid in the interpretation of geologic processes on the moon and as a means for developing improved understanding of soil and rock behavior on the earth.

II. SCOPE OF WORK AND OUTLINE OF FINAL REPORT

As work proceeded on each of these objectives several specific topics emerged as particularly needing more detailed study, and, consequently, during the later phases of the study efforts were intensively directed at these topics. Thus the trend has been from studies of a braod and general nature within a particular area to the isolation of specific problems and more detailed studies of these problems. This is reflected in the general outline of the 4 volumes constituting this report, as shown below:

VOLUME I

LUNAR SOIL MECHANICS AND SOIL PROPERTIES

Chapter 1. Lunar Soil and Rock Problems and Considerations in Their Solution
(James K. Mitchell)

Chapter 2. Engineering Properties of Lunar Soils
(James K. Mitchell and Scott S. Smith)

Chapter 3. Materials Properties Evaluations from Boulder Tracks on the Lunar Surface
(James K. Mitchell and Scott S. Smith)

Chapter 4. Impact Records as a Source of Lunar Surface Material Property Data
(James K. Mitchell, Donald W. Quigley, and Scott S. Smith)

Chapter 5. Lunar Stratigraphy as Revealed by Crater Morphology
(Francois E. Heuzé and Richard E. Goodman)

Chapter 6. Geochemical Studies
(I. S. E. Carmichael and J. Nicholls)

Appendix. Library of Lunar Surface Exploration Materials
(Francois E. Heuzé)

VOLUME II

APPLICATION OF GEOPHYSICAL AND GEOTECHNICAL METHODS TO LUNAR SITES EXPLORATION

—

VOLUME III

PRELIMINARY STUDIES ON SOIL/ROCK ENGINEERING PROBLEMS RELATED TO LUNAR EXPLORATION

C H A P T E R 1

THE NX-BOREHOLE JACK FOR ROCK DEFORMABILITY MEASUREMENTS

by

Richard E. Goodman, Tranh K. Van, and Francois E. Heuzé

CHAPTER 1

THE NX-BOREHOLE JACK FOR ROCK DEFORMABILITY MEASUREMENTS

(Richard E. Goodman, Tranh K. Van, and Francois E. Heuzé)

I. INTRODUCTION

For rational design of foundations one must determine the expectable displacements. This requires knowledge of the deformation-pressure relationships for all the materials in the region of influence of the structure. It is the practice on earth, to obtain a complement of samples from the full volume of affected soils and rocks and to measure their properties in laboratory consolidation or compression tests. A developing but competing art makes it possible on earth to measure the compressibility directly in the field. On the moon it is not so convenient to return samples for meaningful deformability tests as the environment and structural system are difficult to preserve. Therefore the in situ testing art must be invoked.

As described in Volume 2, Chapter 4, a number of instruments have been built to measure rock and soil deformability in boreholes. These were grouped under the headings dilatometers, jacks, and penetrometers. It is proposed that such devices be considered for investigation of sites on the moon. The following discussion explains how data from such tests can be used to determine the deformability properties of the soil or rock.

Particular attention is given to the borehole jack developed by Goodman et al., 1968, as it seems well suited for the purposes and constraints of the lunar program. This instrument is presented in Figures 1a to 1d.

II. INTERPRETATION OF FIELD DATA

The result of deformability testing in a borehole of diameter d is a curve of applied pressure Q versus diametral deformation u_d. By cycling the load, maintaining the load for extended periods, and using other test procedures common in rock engineering studies, valuable qualitative conclusions can be drawn about the rock properties in addition to quantitative information. If the Poisson's ratio of the rock (ν) is assumed or

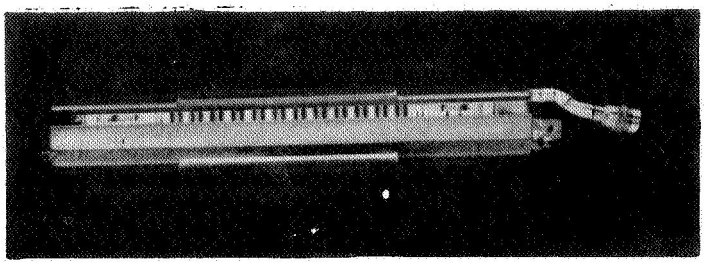

FIGURE 1-1a. NX BOREHOLE PLATE BEARING TEST DEVICE.

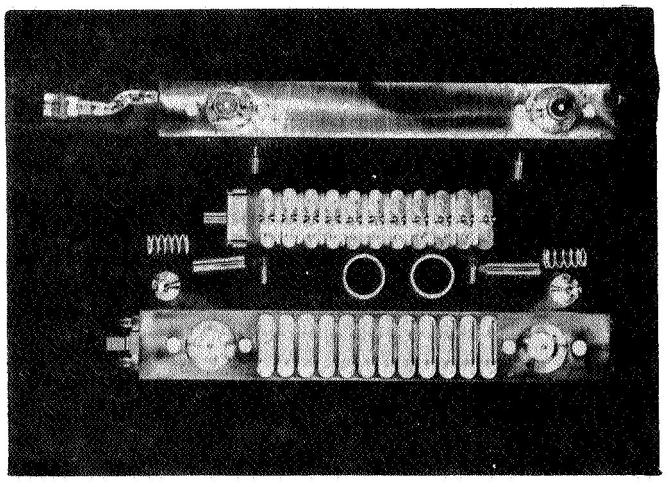

FIGURE 1-1b. DEVICE DISASSEMBLED.

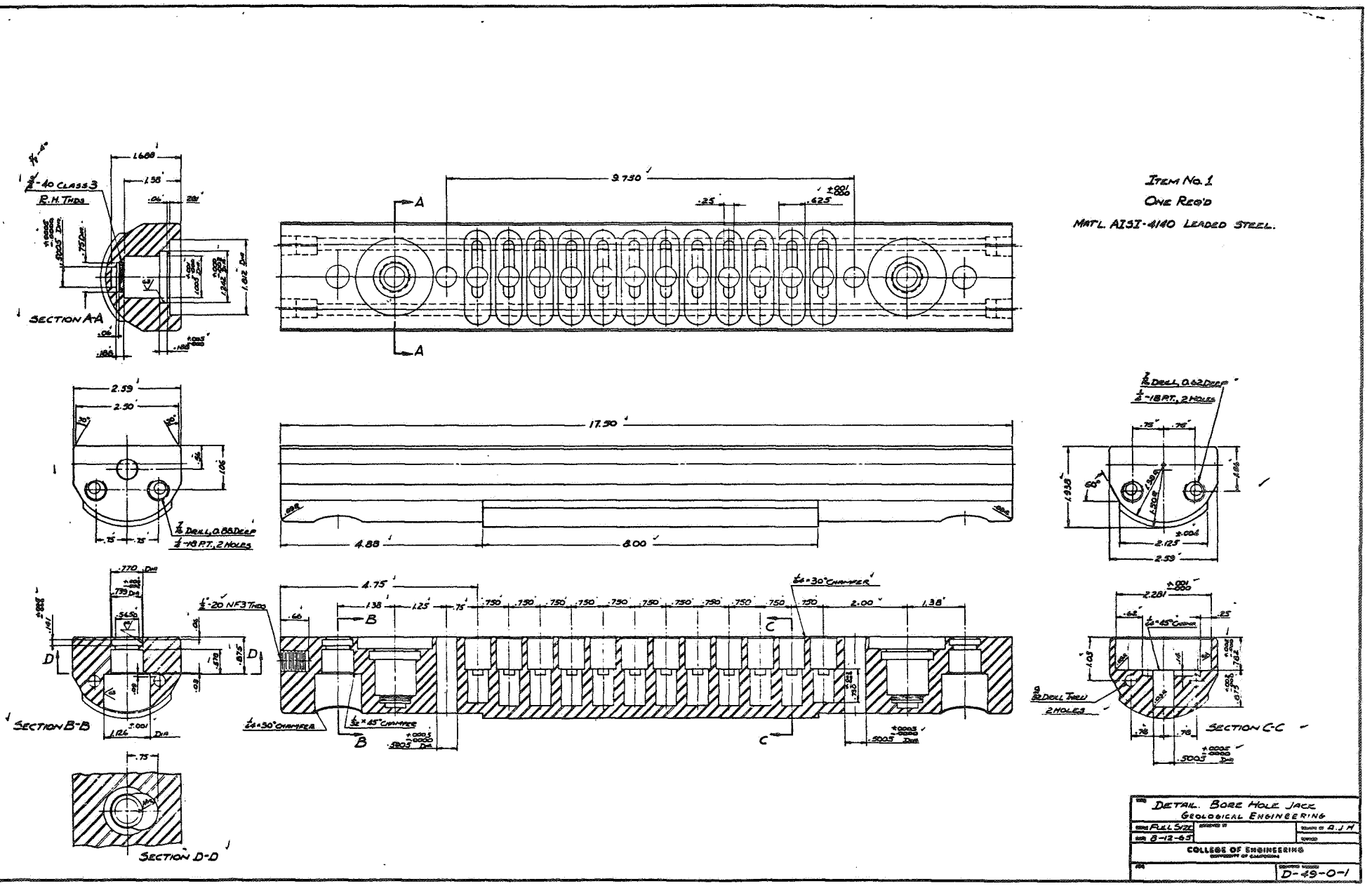

FIGURE 1-1c.
BOREHOLE JACK DETAIL

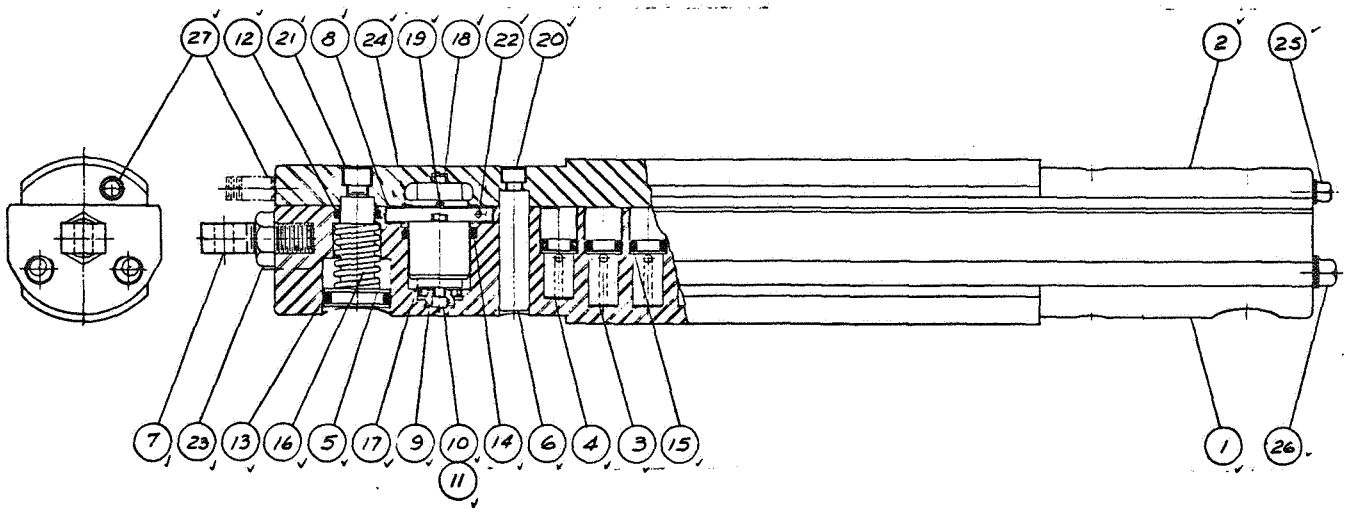

Item No.	Quantity	Drawing No.	Description
1	1	D-49-0-1	
2	1	C-49-0-2	
3	10	C-49-0-3	
4	2		
5	2		
6	2		
7	1		
8	2	B-49-0-4	
9	2		
10	2		
11	2		
12	2		No. 622711 O Ring Rubber
13	2		No. 622717
14	2		No. 622719
15	12		No. 622726
16	2		3/4" O.D. x 15 Ga. (0.072 Dia) Steel Wire Springs 16 Active Coils with Inactive End Coils, 1 1/2 Feet Length
17	2		Schonstedt Diff. Transformer
18	2		Core
19	10		No. 4-40 x 3/16 Long Allen Hd. Scrs. Steel
20	2		1/2-20 x 5/16 Long Stainless Steel
21	2		5/16-18 x 3/4 Long
22	4		No. 6-32 x 3/16 Lg. Allen Hex-Socket Set Scr. Stainless Steel
23	1		1/2-20 Jam Nut Steel
24	2		15/16 I.D. x 1 1/8 O.D. x 1/32 Thick Gasket
25	1		1/8-27 P. Plug Steel
26	2		1/4-18 P. Plugs
27	1		1/8 St. Pipe Nipple, 1" Long T.B.O. Brass

Assembly Bore Hole Jack
Geological Engineering

Full Size | Drawn by R.J.H | Date 8-12-65 | Checked

College of Engineering
University of California

D-49-0-0

FIGURE 1-1d.

measured, a borehole dilatometer or jack gives an expression for Young's modulus from the ratio of ΔQ to $\Delta u_d/d$ for each load increment as discussed below. The selection of final values of deformation modulus for design purpose, as for other in situ tests, will make use of engineering judgment based in part on results obtained from all tests performed in a comprehensive testing program. An example of this is given in Table 1-4.

A. Borehole Dilatometer Data

An expression for E is easily derived from the thick walled cylinder formulas (Jaeger, 1962) by solving for the displacements under internal pressure Q when the outer radius goes to infinity and the outer pressure is zero. This gives:

$$E = \frac{\Delta Q}{\Delta u_d/d} (1 + \nu) \qquad (1\text{-}1)$$

Even if the rock mass is under initial stress, this approach is still valid unless the rock is highly nonlinear as the displacements on pressuring the dilatometer are due only to the applied load. E will be computed as a tangent modulus along the (ΔQ, Δu) curve (see Figure 1-9). As in any loading test, the lowest values for E are generally obtained at the lowest stress levels and the highest along the linear portion of the load deformation curve at the highest stress level when no fracture or yielding takes place.

B. Borehole Jack Data

Quantitative interpretation of measurements made with borehole jacks involves a more difficult formula because the loading is not continuous over the circumference of the borehole wall. Further, except in the case of Jaeger and Cook's Quadrantal curved jacks (Jaeger, Cook, 1963), the force is directed at an inclination to the normal to the borehole wall at all points except the line of symmetry. The boundary condition to be satisfied is one of constant displacement rather than constant pressure. The steel plates are much stiffer than the rock and will be driven out with very little bending. The boundary pressure will not be uniform and pressure readings will represent an average value over

the steel-rock boundary. However, as will be shown, constant displacement solutions are very little different from constant pressure solutions in this class of problems if the average pressure and average displacement over the plate-rock contact area are used in computations.

1. Radial pressure over diametrically opposed sectors of the borehole wall. The solution to this problem was obtained by Jaeger and Cook (1963) using the complex variable method. The complete derivation is given in the Appendix. The radial displacement (u_r) at an angular distance from the center line of the plate extends from + β to − β (Figure 1-3a) is given by

$$\frac{\pi E}{(1+\nu)} \frac{u_r}{aQ} = -2\beta - \sum_{n=1}^{\infty} \frac{1}{n}\left(\frac{3-4\nu}{2n-1} + \frac{1}{2n+1}\right) \cos 2n\theta \sin 2n\beta \qquad (1\text{-}2)$$

The average displacement of plates of given angle 2 β may be obtained by integration. The resulting formula for E would only apply in the case of jacks with radial applied pressure; as yet there are none. This formula should not be used to interpret uniaxially acting borehole jacks.

2. Unidirectional pressure over diametrically opposed sectors of the borehole wall. This is theoretically the problem posed by the use of uniaxially acting borehole jacks. A unidirectional constant pressure boundary condition from − β to + β may be resolved into a constant radial boundary pressure over the borehole section of width 2 β, and shear and radial pressures distributed sinusoidally over the width 2 β as depicted in the Appendix. In the course of this investigation, a solution was obtained for the sinusoidally varying shear and normal force on the wall (Appendix). Superposition with Jaeger's solution (Equation 1-2) yields the following formula for the radial displacement of a point on the wall at θ from the line of symmetry.

$$\frac{\pi E}{1+\nu}\frac{u_r}{aQ} = 2\beta\left[1 + (3-4\nu)\cos 2\theta\right] + \sum_{m=1}^{\infty}\frac{1}{m}\sin 2m\beta$$

$$\left\{\frac{(3-4\nu)}{2m+1}\cos 2(m+1)\theta + \frac{(3-4\nu)}{2m-1}\cos 2m\theta\right.$$

$$\left. + \frac{1}{2m+1}\cos 2m\theta + \frac{1}{2m-1}\cos 2(m-1)\theta\right\} \qquad (1\text{-}3)$$

The average displacement is found by integrating the horizontal displacement over the vertical component of each are segment in contact with the plate, i.e. from $-\beta$ to $+\beta$. The result, shown fully in Equation A-1-31, Appendix, may be written

$$E = \frac{\Delta Q}{\Delta \bar{u}_d/d} K(\nu, \beta) \qquad (1\text{-}4)$$

where $\Delta\bar{u}_d$ is the average diametral dispacement for a given increment of pressure ΔQ and d is the borehole diameter. Values of $K(\nu, \beta)$ are given in Table 1-1.

III. BOREHOLE JACK TEST — DISCUSSION OF DATA INTERPRETATION

A. Influence of Plate Width

Figure 2a, plotted from Table 1-1 shows the variation of K with change in β, the angle subtended by half the plate width of arc. The quantity K, according to Equation 1-4, is the slope of the line relating E to the ratio of the measured quantities ΔQ and $\Delta u_d/d$. The variation of K with β thus affords a comparison of the sensitivity of jacks designed for different plate widths. The maximum sensitivity — the highest value of K — occurs at values of β about 45° (Figure 1-2a), the width selected in designing the NX plate bearing test device. It should be noted here that for small values of β, corresponding to narrow plates, a punching failure of the rock might take place. However, this would hardly be the case when β is as large as 45°.

TABLE 1-1

VALUES OF K (ν, β) FOR USE IN EQUATION 4 — ANALYTICAL SOLUTION

β	ν: 0	0.05	0.10	0.15	0.20	0.25	0.30	0.35	0.40	0.45	0.50
5.0	0.434	0.433	0.430	0.424	0.417	0.407	0.396	0.382	0.366	0.348	0.327
10.0	0.704	0.703	0.698	0.690	0.678	0.663	0.645	0.622	0.597	0.568	0.536
15.0	0.904	0.903	0.897	0.887	0.873	0.054	0.831	0.803	0.772	0.735	0.694
20.0	1.052	1.051	1.046	1.035	1.019	0.998	0.973	0.942	0.906	0.864	0.818
25.0	1.159	1.159	1.154	1.143	1.127	1.105	1.078	1.045	1.007	0.063	0.914
30.0	1.230	1.231	1.227	1.217	1.201	1.179	1.152	1.119	1.080	1.035	0.985
35.0	1.271	1.274	1.271	1.262	1.247	1.226	1.200	1.168	1.129	1.086	1.036
40.0	1.287	1.291	1.290	1.282	1.269	1.250	1.225	1.195	1.159	1.117	1.069
45.0	1.282	1.288	1.288	1.282	1.271	1.254	1.232	1.204	1.170	1.131	1.087
50.0	1.261	1.268	1.270	1.266	1.257	1.243	1.224	1.199	1.169	1.133	1.092
55.0	1.227	1.236	1.240	1.238	1.232	1.221	1.204	1.183	1.156	1.125	1.088
60.0	1.186	1.197	1.202	1.203	1.199	1.190	1.177	1.160	1.137	1.109	1.077
65.0	1.142	1.154	1.161	1.164	1.162	1.156	1.146	1.132	1.113	1.089	1.062
70.0	1.098	1.111	1.120	1.124	1.125	1.122	1.114	1.103	1.088	1.068	1.045
75.0	1.059	1.073	1.083	1.089	1.091	1.090	1.085	1.076	1.064	1.048	1.028
80.0	1.028	1.042	1.053	1.061	1.064	1.065	1.061	1.055	1.044	1.031	1.013
85.0	1.007	1.022	1.034	1.042	1.046	1.048	1.046	1.040	1.031	1.019	1.004
90.0	1.000	1.015	1.027	1.035	1.040	1.042	1.040	1.035	1.027	1.015	1.000

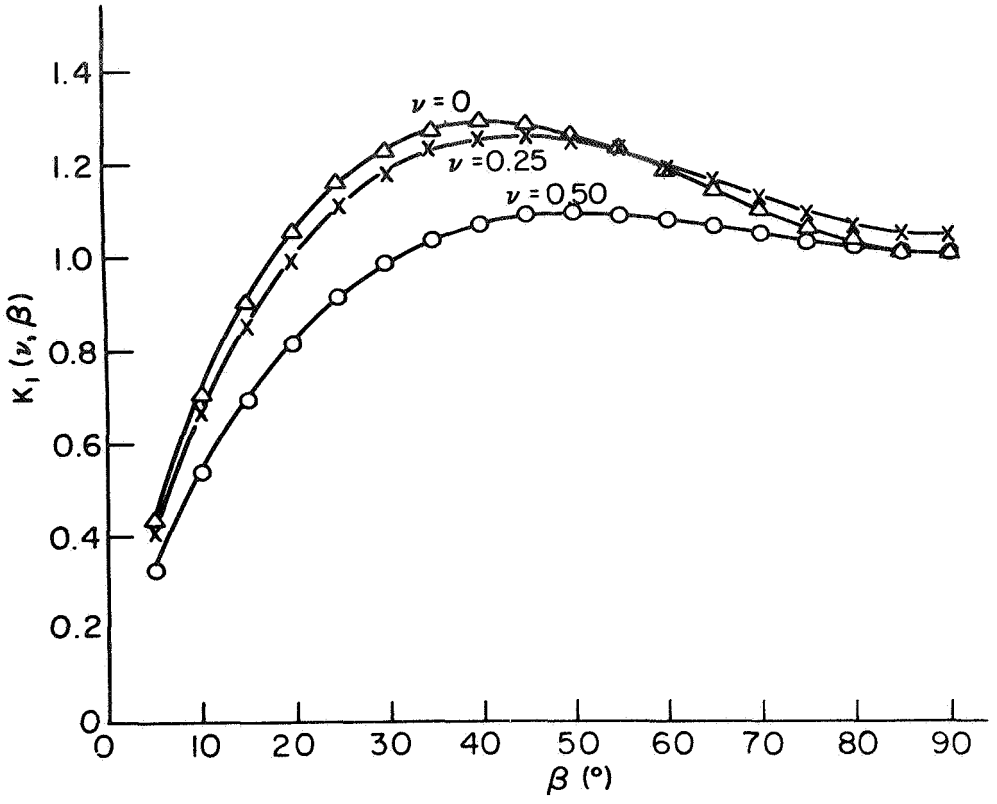

FIGURE I-2a VARIATION OF $K(\nu,\beta)$ WITH RESPECT TO β.

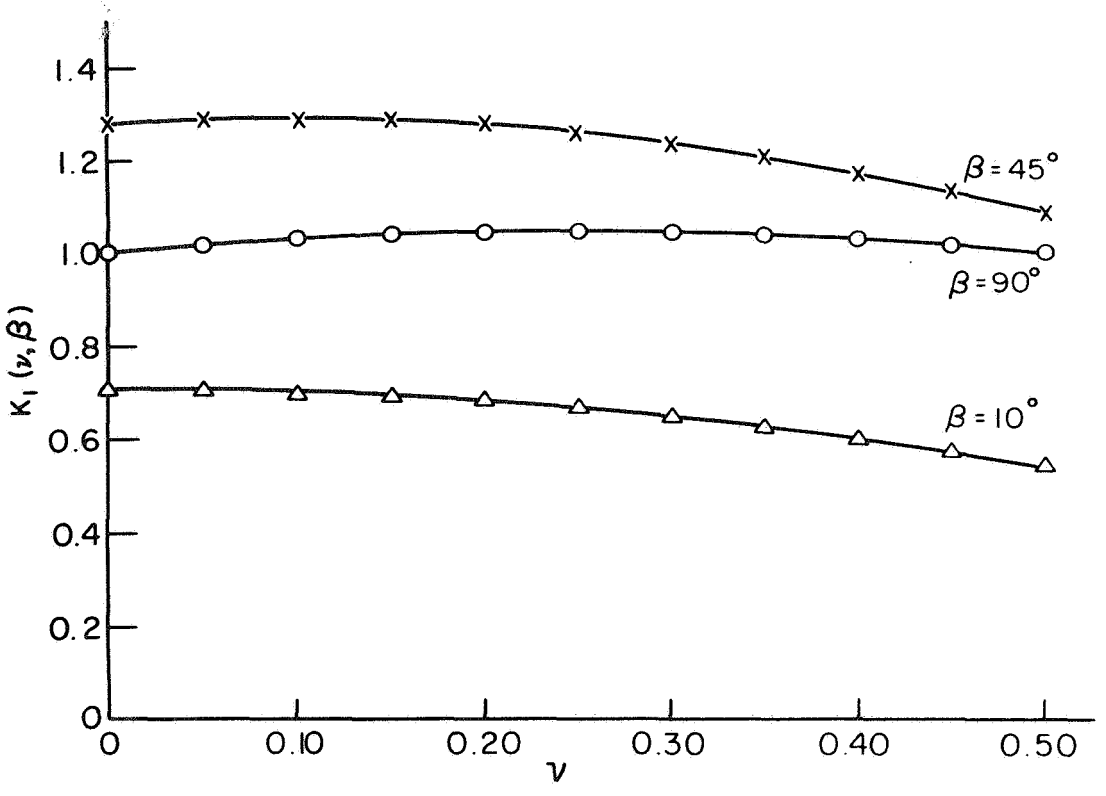

FIGURE I-2b VARIATION OF $K(\nu,\beta)$ WITH RESPECT TO POISSON'S RATIO (ν).

B. Effect of Poisson's Ratio

Figure 1-2b shows that for a given ΔQ and $\Delta u_d/d$, the interpretation of E is fairly insensitive to Poisson's ratio (ν), except at high values of ν. A 50% overestimation in ν, from 0.2 to 0.3, would lead to a 3.25% underestimate of E. If ν were taken as 0.4 rather than the assumed true value of 0.2, and error of 100%, the value assigned for E would be underestimated by 8.50%. As opposed to E, ν is not subject to large discrepancies between field and laboratory values. Thus simple testing on cores retrieved from the borehole would give a value representative enough to preclude such large errors on the Poisson's ratio, hence reducing the error on E to a negligible amount.

C. Effect of Non Linear Rock Properties

Qualitative interpretation of borehole jack or dilatometer data in rock exhibiting non linear stress-strain behavior is entirely appropriate and meaningful. However, as the entire analytical discussion assumes linear elastic relations, quantitative interpretation using these results, even in incremental form, may be erroneous.

D. Effect of Steel Plate

The mathematical solution to the borehole jack problem was derived for a condition of constant horizontal pressure on the inner boundary. In actual fact the boundary condition on the loaded border of the borehole is complex and unknown owing to the unknown coupling between the steel plates and the rock surface. Figure 3a presents a reasonable characterization of the actual boundary condition in the borehole plate bearing device. A uniform hydraulic pressure bears against the inner sides of the plates. Except in very hard rock, the plates are so much stiffer than the rock as to be driven outward with little bending. The result is a nearly constant horizontal displacement of the rock border; other components of displacement may be considered to exist and be unequal according to the friction and Poisson's ratio contrast between the steel and rock.

To assess the significance of this departure from the assumed boundary condition, constant displacement and constant pressure solutions were compared for $\nu = 0.25$ using the method of finite element analysis in

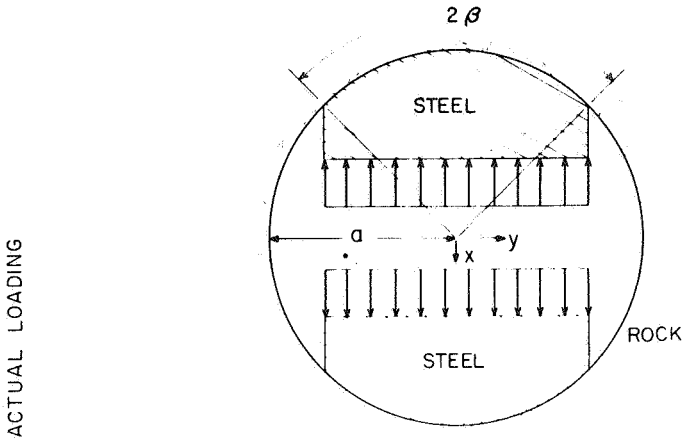

1-3 a ACTUAL BOUNDARY CONDITION

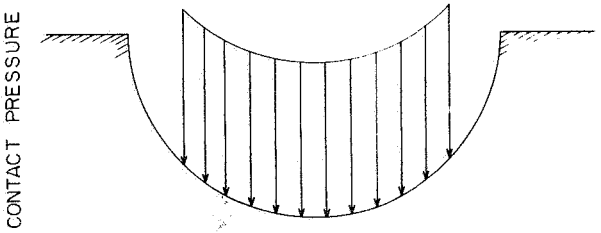

1-3 b. CONSTANT PRESSURE = 10,000 PSI

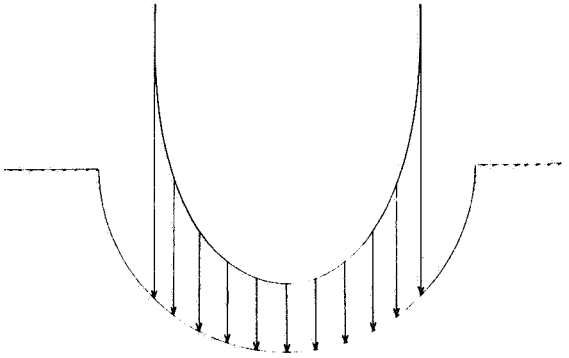

1-3 d CONTACT PRESSURE RESULTING FROM 3e.

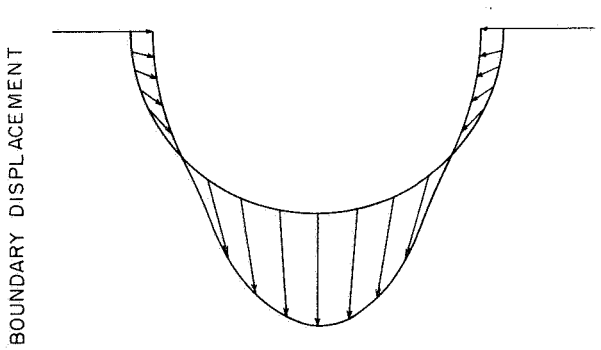

1-3 c. CONTACT DISPLACEMENT RESULTING FROM 3b

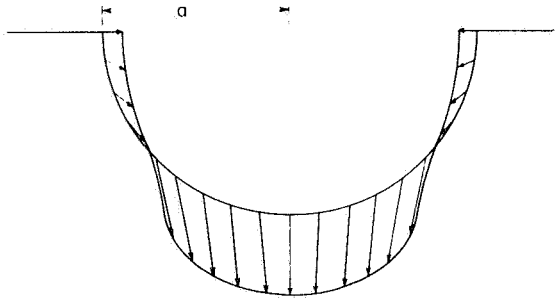

1-3e. CONSTANT DISPLACEMENT $U_x = 0.01a$

FIGURE 1-3 COMPARISON OF CONSTANT PRESSURE AND CONSTANT DISPLACEMENT SOLUTIONS WITH PLANE STRAIN REPRESENTATION OF JACK PROBLEM

$E = 1.0 \times 10^6$ PSI

$\nu = 0.25$

SCALE OF DISPLACEMENT

0 $10^{-2}a$

SCALE OF PRESSURE

0 5000 PSI

plane strain. A fine mesh was used with 775 nodal points and 720 elements. The pressure distribution and displacement vectors along the wall of the borehole are compared for the constant pressure and constant displacement solutions, in Figures 1-3b, c, and 1-3d, e, respectively.

The procedure consists of inputing a constant pressure (or constant X displacement) along the boundary jack-borehole, computing the average X displacement (or pressure) from the output, and using the average value obtained in Eq. 1-1. For $\beta = 45°$ and $\nu = 0.25$, one obtains $K = 1.250$ for the constant X displacement case and $K = 1.235$ for the constant pressure case as compared to $K = 1.254$ for the exact analytical solutions. The constant X displacement case is believed to be the more representative of actual field behavior and its simulation by finite element analysis gave the closest result to exact solutions ($K = 1.250$ versus $K = 1.254$). This is the extent of the finite element approximation.

E. Effect of Finite Test Length

The plane strain solution assumes an infinite test length. In actual fact the NX borehole plate bearing device has a length to diameter ratio of 8"/3". To calculate the effect of the finite plate is a difficult three dimensional problem in prismatic space which could not be solved in closed form.* However, an estimate of the end effect was obtained by performing a three dimensional finite element analysis using a new computer program developed by Professor E. L. Wilson (1967). In this approach, a load of finite length is applied to a portion of a longer space whose cross section is constant. The variation of load along the length of the space is achieved by Fourier expansion making repeated cumulative passes through the problem.

Figure 1-4 gives the variation of displacement at the border of the borehole over the width and length subjected to uniform pressure ($\nu = 0.25$). The value of K corresponding to the average displacement under the loaded

---

*The related three dimensional problem of a hydrostatic pressure of finite length 2 c in a circular hole of radius a was solved by Tranter in 1946 (Quarterly of Applied Mathematics, vol. 4, p. 298). The three dimensional effect was 37% for c/a = 0.5 and was decreasing rapidly with increased load length. In the NX plate bearing test, c/a = 2.67.

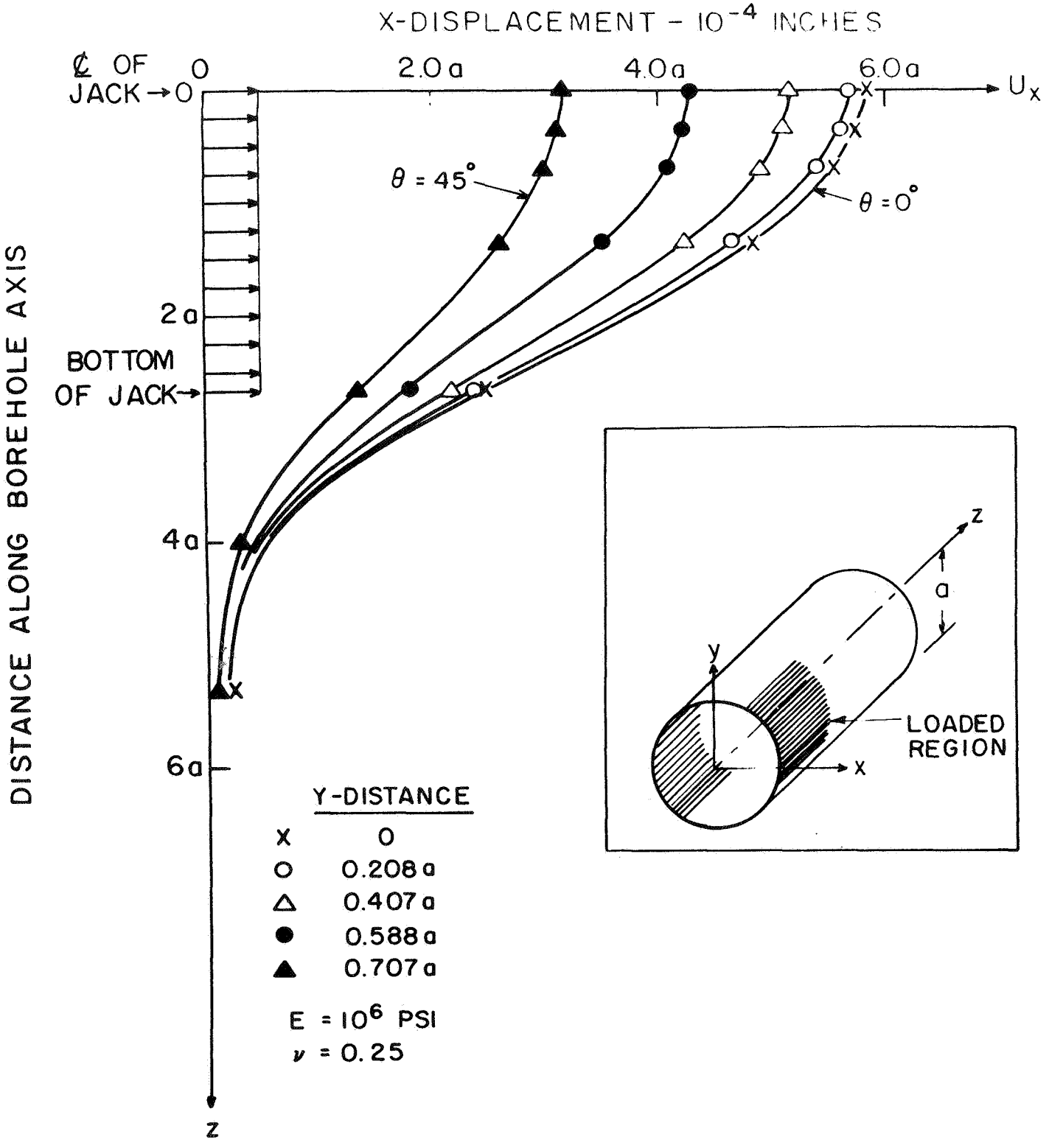

FIGURE I-4 VARIATION OF X-DISPLACEMENT ALONG THE BOREHOLE (z DIRECTION) AT DIFFERENT POINTS AROUND THE WALL OF THE BOREHOLE. PRISMATIC-SPACE - CONSTANT PRESSURE = 375 PSI.

area is 1.06. The corresponding value from finite element analysis of the plane strain approximation is 1.23. Thus the finite length may be taken into account by reducing by 14% values of E derived from Eq. 1-4 and Table 1-1, i.e.

$$E = 0.86\ K(\nu)\ \frac{\Delta Q}{\Delta u_d/d} \qquad (1\text{-}5)$$

In the NX borehole plate bearing device, d = 3 inches, and Q is 93% of the hydraulic pressure Q_h. Putting these values in Equation 1-5 yields the following equation for interpretation of field data in tests with this instrument.

$$E = 2.40\ K(\nu)\frac{\Delta Q_h}{\Delta u_d} \qquad (1\text{-}6)$$

TABLE 1-1

Values of Constants in Equation 1-6

ν	0	0.05	0.10	0.15	0.20	0.25	0.30	0.35	0.40	0.45	0.50
$K(\nu)$	1.38	1.29	1.29	1.28	1.27	1.25	1.23	1.20	1.17	1.13	1.09
2.40 $K(\nu)$	3.07	3.10	3.10	3.07	3.05	3.00	2.95	2.88	2.81	2.71	2.62

F. Rock Stress with the Borehole Jack

The complex variable method leads to series formulas for the stress components in the rock, as presented in the Appendix. The thrusting apart of the borehole by the action of the jack leads to a tangential tension on

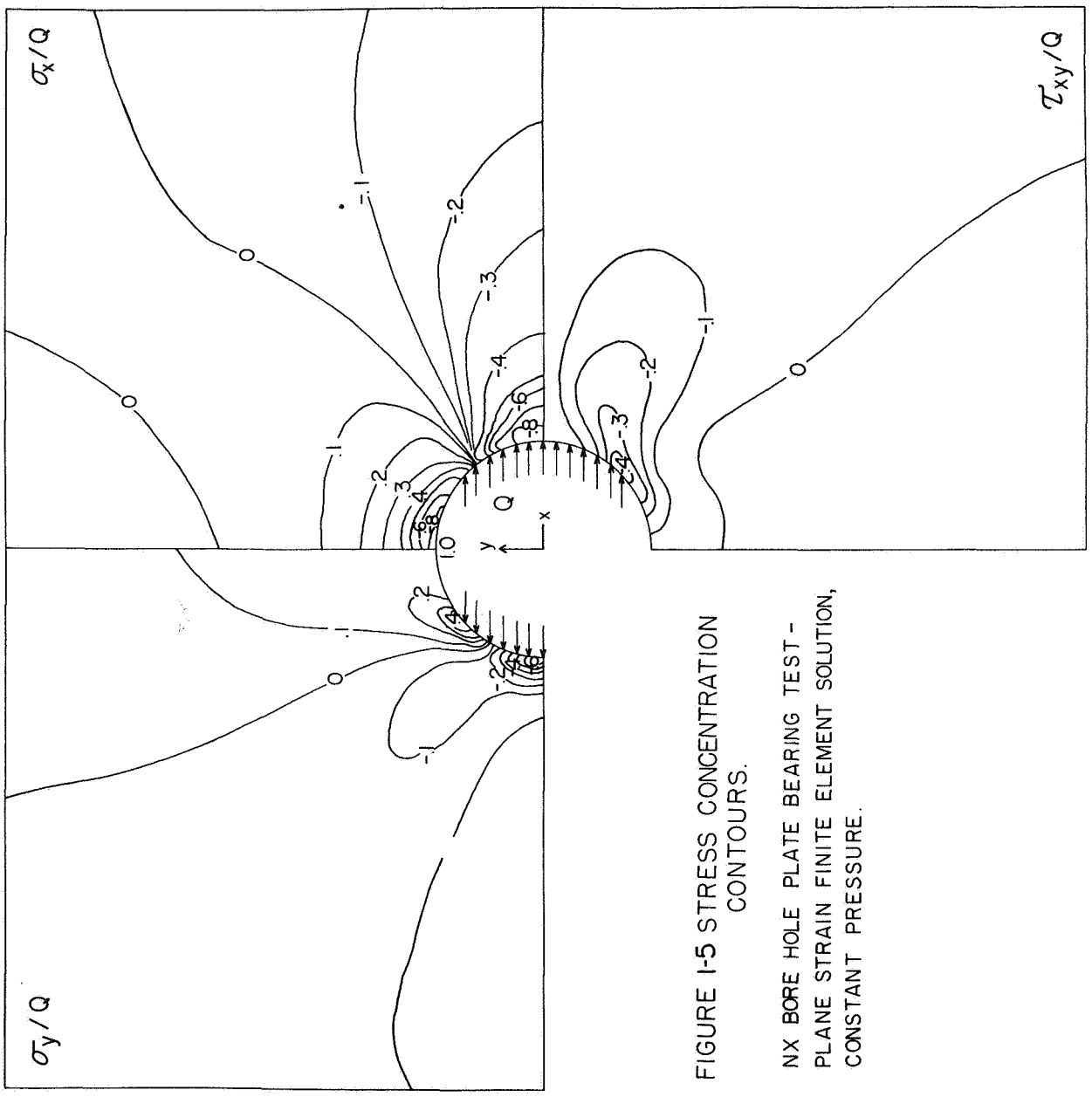

FIGURE I-5 STRESS CONCENTRATION CONTOURS.

NX BORE HOLE PLATE BEARING TEST - PLANE STRAIN FINITE ELEMENT SOLUTION, CONSTANT PRESSURE.

the wall of the borehole at $\theta = 90°$

$$\sigma_\theta = -4\beta\frac{Q}{\pi}$$

For the NX borehole plate bearing device, $\beta = \pi/4$ giving a tangential stress concentration at $\theta = 90°$ of -1.0. The onset of tensile cracking at this point could be used as a measure of the tensile strength of the rock if a borehole camera is used concurrently. From Equation 1-A-32 (Appendix), one also obtains at $\theta = 0°$, $\sigma_\theta = 0.875\ Q$ (compressive).

The stresses around the borehole expressed as a concentration of the jack pressure are presented in Figures 1-5a, b, and c.

G. Influence of Possible Crack Formation

In all that precedes, the rock has been assumed to be homogeneous, isotropic, and linearly elastic. Moreover, no failure criterion has been considered around the borehole. However, owing to the magnitude of stresses which the jack can induce, superimposed onto the in situ stress concentrations, it is not unlikely that cracking might develop around the borehole particularly in soft or weak rocks. Cracks could be originated and propagated primarily in those regions where high tensile stresses are found to develop; the critical ones will be the tangential stresses. Then, upon data analysis, corrections shall be introduced to take care of the apparent reduction in the computed modulus of elasticity to obtain the true value for intact rock. Both concepts presented above are discussed.

The complete tangential stress field at selected points (on the walls of the borehole and in planes of principal stresses) around the borehole can be readily obtained by superposition of the effects of in situ biaxial stress field (S, T) and of jacking (Q). Figure 1-6a gives the tangential stress concentration factors. Depending upon the ratio S/T, the stress pattern before jack pressurization can take different forms. They are shown on Figure 1-6b assuming that $S/T = N = \nu/(1-\nu)$ (lateral constraint). If S and T have been actually measured, the proper

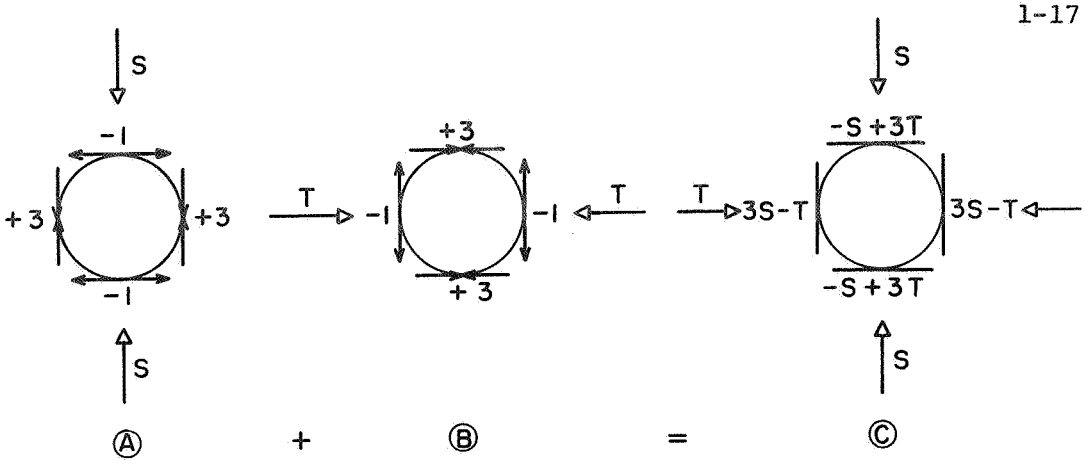

a) TANGENTIAL STRESS CONCENTRATION FACTORS AROUND A BOREHOLE IN A BIAXIAL STRESS FIELD.

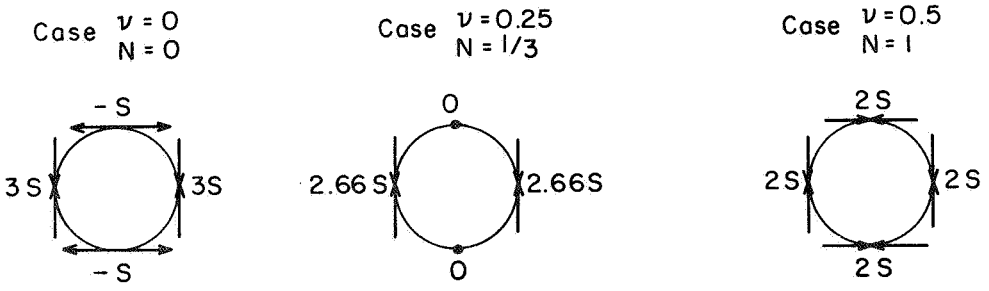

b) TANGENTIAL STRESSES AROUND BOREHOLE — NO JACKING.

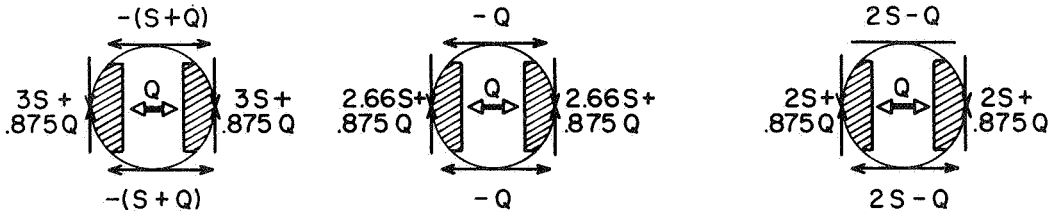

c) JACKING IN DIRECTION OF MINOR PRINCIPAL STRESS.

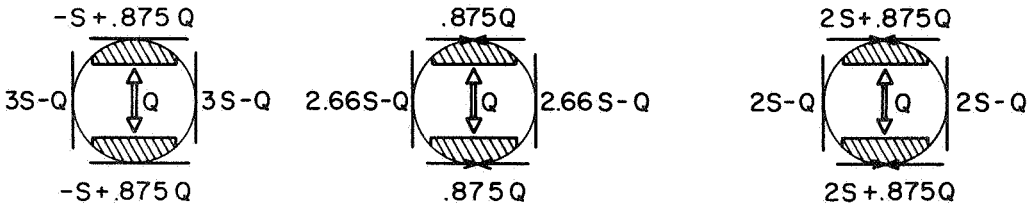

d) JACKING IN DIRECTION OF MAJOR PRINCIPAL STRESS.

S = MAJOR PRINCIPAL STRESS (positive in compression)
T = MINOR PRINCIPAL STRESS (positive in compression)
Q = JACK PRESSURE (positive)

FIGURE 1-6
CUMULATIVE STRESS CONCENTRATION FACTORS AROUND BOREHOLE

value will then be used. Upon application of a jack pressure Q, the additional tangential stress induced is for $\beta = 45°$ at $\theta = 90°$, $\sigma_\theta = -Q$ and at $\theta = 0°$, $\sigma_\theta = 0.875\ Q$. Accordingly, the complete tangential stress pattern at the selected points is shown on Figures 1-6c and 1-6d when jacking takes place in the direction of either principal stress. These are the two extreme cases in terms of tangential stress magnitude. It can be seen that the most unfavorable situation is when jacking takes place in the direction of the minor principal stress. High tensile tangential stresses will then be induced in the plane perpendicular to the direction of jacking, and the lower the Poisson's ratio of the rock, the higher their magnitude.

In the eventuality of crack formation in a plane perpendicular to the direction of jacking, the observed displacement of the jack plates will be greater than the one taking place in an intact body. Thus, the modulus of elasticity computed from load-deformation curves will be lower than if no crack is initiated. Evaluation of the required correction on E was attempted by simulation technique. The constant X displacement finite element model was used according to previous conclusions. Cracking was simulated by allowing no tensile strength for a certain distance d from the borehole along the plane perpendicular to the direction of jacking. Three cases were considered:

$\sigma = d/4$ (crack extending to a half radius distance)

$\sigma = d/2$ (crack extending to a one radius distance)

$\sigma = 2.5\ d$ (simulates a half infinite medium for all practical purposes)

The results are compared in Table 1-3 with the case of no cracking.

Unless indicated by a break, or yield point, in the load deformation curve, cracking at depth in a borehole would be monitored by means of borehole camera, but its extent from the wall inside would be extremely difficult to measure. However, from Figure 1-5b, one can

TABLE 1-3

Influence of Possible Crack Formation

Length of Crack	K	Variation in K	Apparent Decrease in E
0	1.250	+ 0	—
d/2	1.410	+ 13%	− 13%
d	1.553	+ 24%	− 24%
2.5 d	1.614	+ 29%	− 29%

see that at a distance, d = 1 radius, the maximum tensile tangential stress induced by jacking has decreased to 0.1 Q (maximum value = 930 psi). Moreover, within a short distance from the borehole, the in situ stress field is again compressive. Thus it is very unlikely that a crack could propagate beyond between 1/2 and 1 radius from the borehole even in the weakest rock. Accordingly, the corresponding maximum correction to be introduced in the computed modulus of elasticity will probably never exceed 15%. This is well within the limits of accuracy required for engineering purposes knowing that usually results of any test are checked against results obtained by other methods. In case of jacking across a joint intersecting the borehole, the required correction could reach close to 30% and it is suggested that a close examination of jacking explacements be made before actual testing in order to avoid the influence of major discontinuities in the rock mass.

H. Influence of Wall Roughness and Roundness

Other investigators (Suzuki, 1967; Agarrval, 1967) have analyzed the influence of borehole wall roughness and roundness on the accuracy of stress determinations from borehole deformations. They conclude that with modern diamond drilling equipment and honing devices the morphology of the boreholes enable accurate measurements. In the case of jack testing, crushing of asperities might take place at the beginning of loading

but the modulus of deformation is obtained from the linear portion of the load deformation curve which corresponds to a uniform loading. After Suzuki (1967), roughness can be limited to about 10^{-3} inches, whereas, plate displacement is of the order of several 10^{-2} inches, so that for practical purposes, no correction will have to be introduced.

I. The Size of Borehole Jack Tests

A borehole jack produces nonhomogeneous stress and displacement fields in the rock around the borehole. Figures 1-5a, b, and c give the rate at which the applied pressure decays with depth, and Figure 1-7 presents the decay of displacement with depth. The size of the tests can be expressed by the volume of rock significantly stressed, say to a minimum of 1,000 psi, and within which most, ca. 90% of the displacement has occurred. At a plate pressure of 9,000 psi this volume extends about 4.5 inches deep from the wall of the NX borehole. Thus, the test may be considered as operating on an irregularly shaped rock domain roughly one foot in maximum extent. It is much larger than laboratory tests, and somewhat smaller than conventional plate bearing tests conducted in adits.

IV. COMPARISON OF BOREHOLE JACK AND OTHER IN SITU TESTS

NX borehole plate bearing tests were conducted in three underground test chambers where extensive in situ testing programs had been completed or were in progress. These were at the Tehachapi tunnel near Bakersfield (California Department of Water Resources); Dworshak dam near Orofino, Idaho (Walla Walla District, U. S. Corps of Engineers); and the Crestmore mine near Riverside, California (American Cement Co.). The equipment used in these tests included the NX borehole plate bearing device, two Schaevitz servo indicators, a double acting 10,000 psi hand pump, and Bourdon pressure gages, as depicted in Figure 1-8.

At the test gallery of the Tehachapi project an adit to the discharge tunnel, the rock is a closely fractured diorite gneiss with seams of clay derived from the rock by hydrothermal alteration. Several hard, fresh pieces of core were obtained in drilling the NX holes for the borehole plate bearing tests but the overall recovery was only fair. Four borehole jack tests were conducted in two horizontal holes.

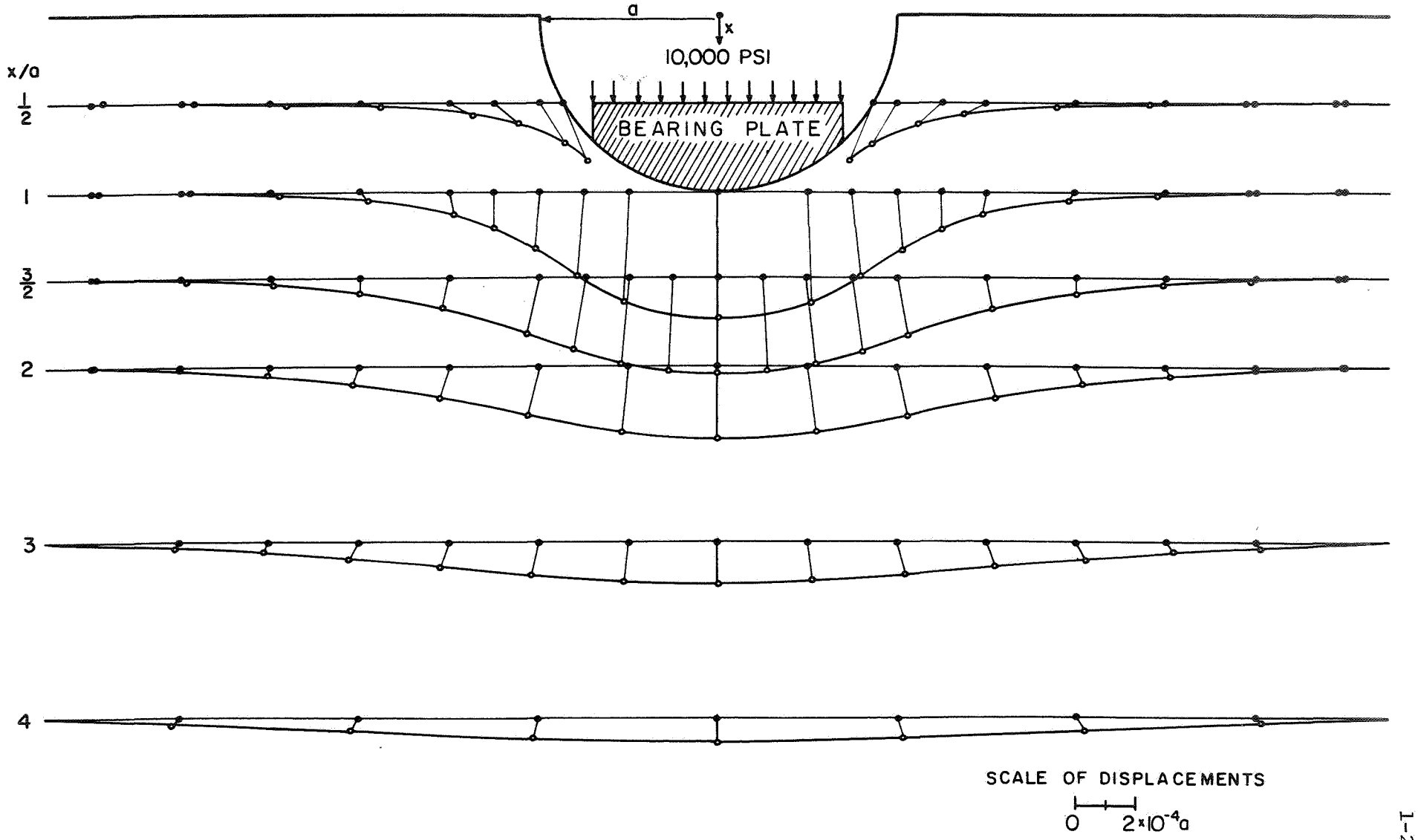

FIG. I-7 DISPLACEMENTS OF ROCK UNDER 10,000 PSI LOAD BY BORE HOLE JACK.
ELASTIC MODULUS OF ROCK = 1.0×10^6 PSI.

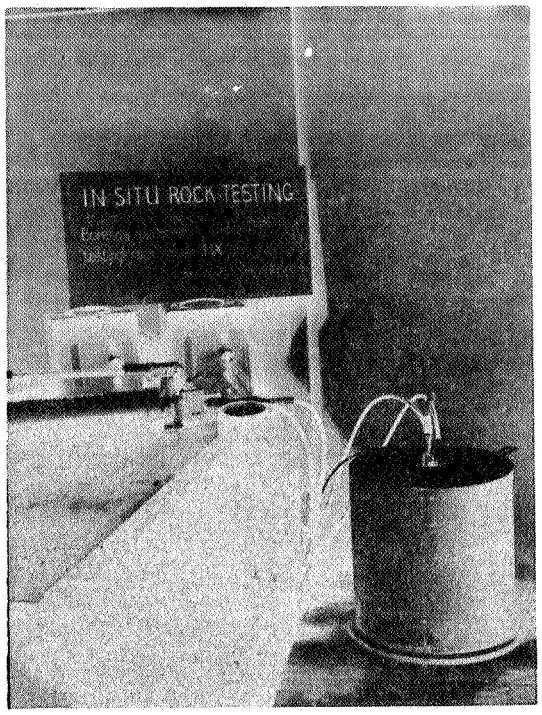

FIGURE 1-8. COMPLETE EQUIPMENT FOR NX BOREHOLE PLATE BEARING TEST. THE APPROXIMATE DIMENSIONS OF THE VOLUME OF ROCK UNDER TEST IN SITU IS INDICATED BY THE CONCRETE CYLINDER.

In situ tests included stress measurements, seismic measurements, and plate bearing tests. Four plate bearing tests were performed; and analyses were made of the data assuming both uniform and rotational deflections, as discussed by Stroppini and Kruse (1964) for similar tests at Oroville. Figure 9a presents a typical pressure versus diametral displacement curve for the borehole jack tests at this location. The average value of E from plate bearing tests was 700,000 psi; the average value of E from borehole jack tests was 840,000 psi in the same pressure range.

The Dworshak dam tests were conducted in a test gallery employed previously by Shannon and Wilson (1965) for a comprehensive program of in situ rock tests. The rock at this site is a massive to moderately jointed epidote quartz-diorite gneiss. The in situ tests included plate bearing test, a chamber test, and seismic measurements.

There was great scatter in the results of plate bearing tests; the mean modulus of elasticity in plate bearing was 3.4 million psi with individual results ranging from 500,000 psi to 5 million psi. Fourteen borehole jack tests were conducted in eight boreholes, three of which were water filled. The average modulus from these tests was 2.1 million psi, with little scatter. A typical curve of pressure versus displacement for borehole jack tests is shown in Figure 1-9b.

An extensive program of in situ tests were completed by Heuzé and Goodman (1967) at Crestmore mine, an underground room and pillar mine in massive, coarse, crystalline marble. In situ tests included flat jack measurements, plate bearing tests, and field seismic measurements. Borehole jack tests were conducted in two horizontal boreholes at the site of the flat jack emplacements. The modulus of elasticity values computed from the load deformation curves on pressuring the flat jacks averaged 1.8 million psi. The borehole jacks gave an average value of 1.5 million psi for E. A typical curve of plate pressure versus diametral displacement for the borehole tests is given in Figure 1-9c.

Table 1-4 is a summary and comparison of test results from the three areas.

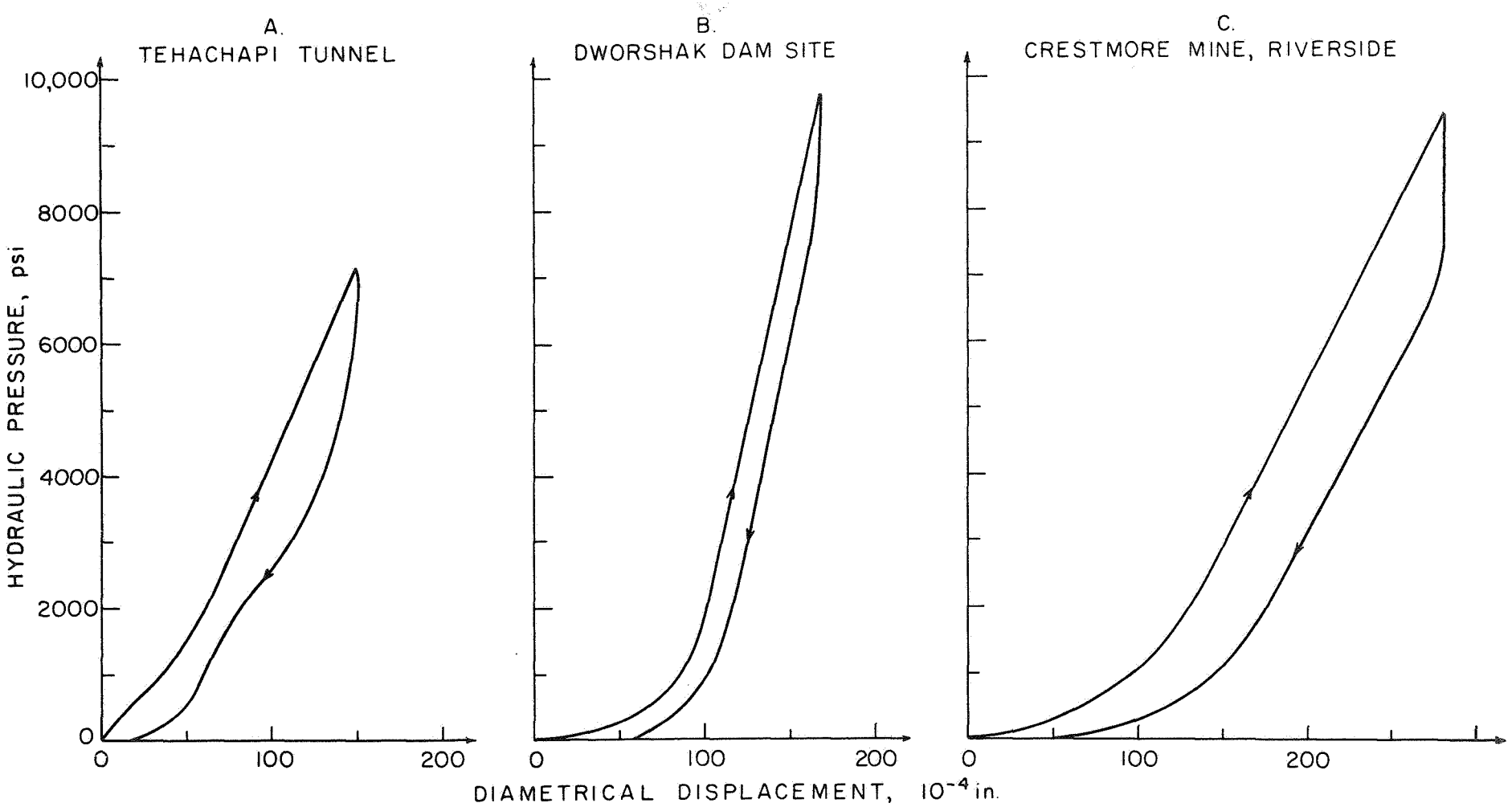

FIGURE I-9 PRESSURE DEFORMATION CURVES FOR FIELD TESTS WITH NX PLATE BEARING DEVICE.

At each of the sites, E was measured, additionally, in unconfined compression tests on NX core specimens in the laboratory. These values were, in all cases, considerably higher than the results of static tests in situ — by a factor of 3 or more. This discrepancy between field and laboratory values is a common one in rock testing. Laboratory testing is usually conducted on solid samples which are not fully representative of the rock mass with its defects. The results of the borehole jack tests were comparable to those of other in situ tests.

Borehole jack tests are well suited to measurements of rock deformability at engineering sites. The tests are easier and less costly to conduct than plate bearing, flat jack, and other in situ techniques; thus many more measurements can be made. Furthermore, being conducted in drill holes, rock volumes remote from the surface can be tested. These facts allow one to establish the attributes of the rock mass quantitatively and qualitatively in every rock member reached by a work. The values obtained from these tests in three earth rock engineering cases discussed herein were comparable to values obtained by other more costly in situ techniques.

V. FURTHER RESEARCH

This report has reviewed current knowledge on determination of the in-situ deformability of rocks and soils. In principle, it is also possible to load the borehole walls to failure with borehole devices to determine the soil or rock strength. The load-deformation information to failure could then be used to determine the bearing capacity and other required design parameters of lunar materials.

In order to determine the strength parameters of soil or rock from a borehole test it is necessary to know: the distribution of contact pressure achieved by the loading device; the state of stress induced into the material at different stress levels; the actual load deformation characteristics of the material under homogeneous stresses; failure criteria; failure mechanism; and the geometry of the problem (length and width of bearing plate, depth of hole, and variation of hole diameter). To obtain this information both theoretical and experimental studies are required.

TABLE 1-4

SUMMARY OF TEST RESULTS

COMPARISON OF IN SITU, CORE, AND BOREHOLE JACK TESTS

Site	Rock Type	Poisson's Ratio	Young's Modulus, 10^6 psi			
			Unconfined Compression (laboratory average)	Plate Bearing (in situ)	Flat Jack* (in situ)	Bore Hole Jack* (in situ)
Tehachapi Tunnel	Diorite gneiss fractured and seamy	0.35	11.3	0.53 to 0.83		0.61 to 1.03
Dworshak Dam	Granite gneiss; massive to moderately jointed	0.20	7.5	0.5 to 5.0		1.54 to 2.70
Crestmore Mine	Marble; massive	0.25	6.9	1.74 to 2.72	1.79 to 2.98	1.35 to 1.95

*in the same pressure range 0 — 3,000 psi

REFERENCES

1. Agarrval, R. (1967), "Sensitivity Analysis of Borehole Deformation Measurements of In Situ Stress Determination when Affected by Borehole Excentricity," Proceedings 9th Symposium on Rock Mechanics, Golden, Colorado, April.

2. Heuzé, F. E. and Goodman, R. E. (1967), "Mechanical Properties and In Situ Behavior of the Chino Limestone, Crestmore Mine, Riverside, California," Proceedings 9th Symposium on Rock Mechanics, AIME, April.

3. Jaeger, J. C. (1962), Elasticity, Fracture and Flow, Methuen and Co., London, 2nd. ed.

4. Jaeger, J. C. and Cook, N. G. W. (1963), "Theory and Application of Curved Jacks for Measurement of Stresses," International Conference on State of Stress in the Earth's Crust, Santa Monica, California, May, Elsevier Press (Ed. Judd).

5. Shannon and Wilson, Inc. (1965), "In Situ Rock Tests for Dworshak Dam Site," January 25.

6. Stroppini, E. W. and Kruse, G. H. (1964), "Discussion of 'Foundation Modulus Tests for Karadj Arch Dam'" by Waldorf, et al., Journal Soil Mechanics and Foundation Division, Proceedings, ASCE, Vol. 90, No. SM 2, March.

7. Suzuki, K. (1966), "Fundamental Study of Rock Stress Measurements by Borehole Deformation Method," Proceedings 1st Congress of Int'l. Soc. Rock Mechanics, Vol. II.

8. Wilson, E. L. (1967), "Stress Analysis of Prismatic Solids," SESM Report, Dept. Civil Engineering, University of California, Berkeley.

SYMBOLS

d	Borehole diameter (in)
E	Modulus of elasticity (Young's Modulus) (psi)
K	Constant (for a given ν and β)
Q	Applied unidirectional pressure = 0.93 Q_h (psi)
Q_h	Hydraulic pressure (psi)
U_d	Diametral borehole deformation (in)
β	Half plate width (degrees)
ΔQ	Increment load (psi)
ΔU_d	Incremental deformation (in)
ν	Poisson's Ratio

APPENDIX

SOLUTION OF UNIAXIAL STRESS PROBLEM BY COMPLEX VARIABLE METHOD

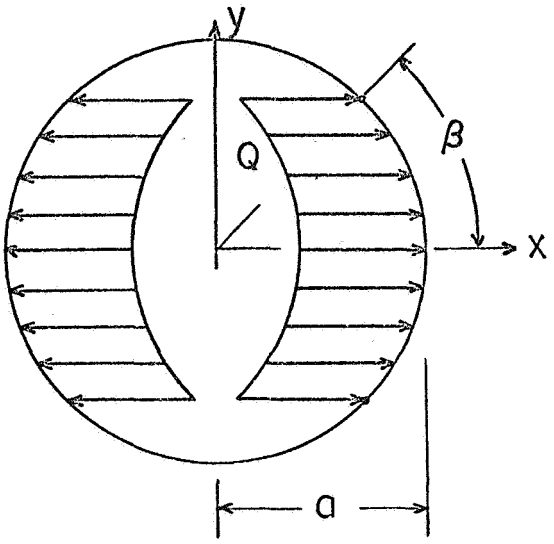

Boundary condition at r = a, $\sigma_y = 0$, and $\tau_{xy} = 0$

$$\sigma_x = \begin{cases} Q & -\beta < \theta < \beta \quad , \quad \pi - \beta < \theta < \beta + \pi \\ 0 & \beta < \theta < \pi - \beta \quad , \quad \pi + \beta < \theta < 2\pi - \beta \end{cases} \qquad \text{1-A-1}$$

At θ from x - axis (Q = 2 p):

$$\begin{aligned} \sigma_r &= p + p\cos 2\theta \\ \sigma_\theta &= p - p\cos 2\theta \\ \tau_{r\theta} &= -p\sin 2\theta \end{aligned} \qquad \text{1-A-2}$$

The problem can be conveniently decomposed into two more simple problems, A and B. Each problem will be solved separately, and the results are added. The displacement relations and the stress relations are expressed in complex forms.

A. UNIFORM STRESS OVER TWO SYMMETRICAL PORTIONS OF THE CIRCULAR BOREHOLE*

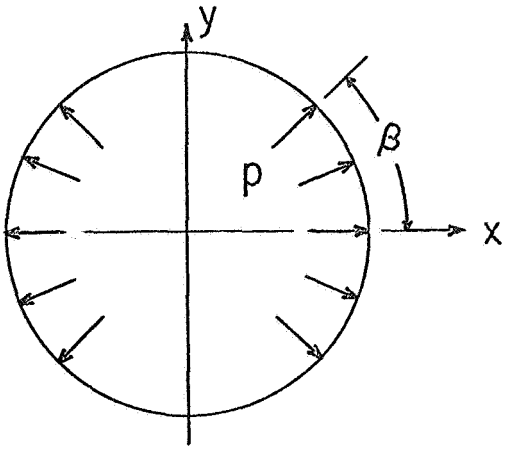

Boundary conditions at r = a

$$\tau_{r\theta} = 0 \qquad \text{1-A-3}$$

$$\sigma_r = \begin{cases} p & -\beta < \theta < \beta \quad , \quad \pi - \beta < \theta < \pi + \beta \\ 0 & \beta < \theta < \pi - \beta \quad , \quad \pi + \beta < \theta < 2\pi - \beta \end{cases} \qquad \text{1-A-4}$$

$$\sigma_r - i\tau_{r\theta} = \sum_{n=-\infty}^{\infty} An\ e^{in\theta} \qquad \text{1-A-5}$$

where

$$An = \frac{1}{2\pi} \int_0^{2\pi} (\sigma_r - i\tau_{r\theta})\ e^{-in\theta}\ d\theta \qquad \text{1-A-6}$$

$$\sigma_r - i\tau_{r\theta} = \phi'(z) + \overline{\phi'(z)} - [\, z\,\phi''(z) + \chi''(z)\,]\ e^{2i\theta} \qquad \text{1-A-7}$$

---

*This problem was first solved by Jaeger and Cook in State of Stress in the Earth's Crust (W. R. Judd, ed.), Elsevier, 1964, p. 381-396.

$$\phi'(z) = \sum_{n=0}^{\infty} a_n z^{-n}$$

$$\chi''(z) = \sum_{n=0}^{\infty} b_n z^{-n} \qquad \text{1-A-8}$$

$$a_0 = b_0 = 0$$

$$\xi a_1 + \overline{b_1} = 0 \qquad \text{1-A-9}$$

Solve for a_n and b_n:

$$\phi'(z) = \sum_{n=0}^{\infty} a_n z^{-n} = \sum_{m=1}^{\infty} \frac{p a^{2m}}{m \pi} \sin 2m\beta \; z^{-2m} \qquad \text{1-A-10}$$

$$\chi''(z) = \sum_{n=0}^{\infty} b_n z^{-n} = -\frac{2\beta p}{\pi} a^2 z^{-2} + \sum_{m=1}^{\infty} \frac{2p a^{2(m+1)}}{\pi} \sin 2m\beta \; z^{-2(m+1)} \qquad \text{1-A-}$$

Determination of Displacement:

$$2G(u_r + i u_\theta) = [\xi \phi(z) - z\overline{\phi'(z)} - \overline{\chi(z)}] e^{-i\theta} \qquad \text{1-A-12}$$

$$2G u_r = \text{Real (R.H.S.)} = -\frac{2\beta p \rho a}{\pi} + \sum_{m=1}^{\infty} \frac{\xi p \rho^{(2m-1)}}{m(1-2m)} a \sin 2m\beta \cos 2m\theta$$

$$- \sum_{m=1}^{\infty} \frac{p \rho^{(2m-1)}}{m \pi} a \sin 2m\beta \cos 2m\theta$$

$$+ 2\sum_{m=1}^{\infty} \frac{p \rho^{2(m+1)}}{\pi(2m+1)} a \sin 2m\beta \cos 2m\theta \qquad \text{1-A-13}$$

$\rho = 1$

$$2 G u_r \frac{\pi}{p a} = -2\beta - \sum_{m=1}^{\infty} \frac{1}{m} \left[\frac{\xi}{2m-1} + \frac{1}{2m+1} \right] \sin 2m\beta \cos 2m\theta \qquad 1\text{-A-14}$$

Stress Determination:

$$\sigma_\theta + \sigma_r = 4 \text{ Real } [\phi'(z)] \qquad 1\text{-A-15}$$

$$\sigma_\theta - \sigma_r + 2i\tau_{r\theta} = 2 [\bar{z}\, \phi''(z) + \chi''(z)]\, e^{2i\theta} \qquad 1\text{-A-16}$$

$$\sigma_\theta \frac{\pi}{p} = -2\beta\rho^2 + 2\sum_{m=1}^{\infty} \frac{1}{m} \rho^{2m} (m\rho^2 - m + 1) \sin 2m\beta \cos 2m\theta \qquad 1\text{-A-17}$$

$$\sigma_r \frac{\pi}{p} = 2\beta\rho^2 + 2\sum_{m=1}^{\infty} \frac{1}{m} \rho^{2m} (m + 1 - m\rho^2) \sin 2m\beta \cos 2m\theta \qquad 1\text{-A-18}$$

$$\tau_{r\theta} \frac{\pi}{p} = 2(1 - \rho^2) \sum_{m=1}^{\infty} \rho^{2m} \sin 2m\theta \sin 2m\beta \qquad 1\text{-A-19}$$

B. THE EXPONENTIAL BOUNDARY CONDITION PROBLEM: $\sigma_r - i\,\tau_{r\theta} = p\,e^{2i\theta}$

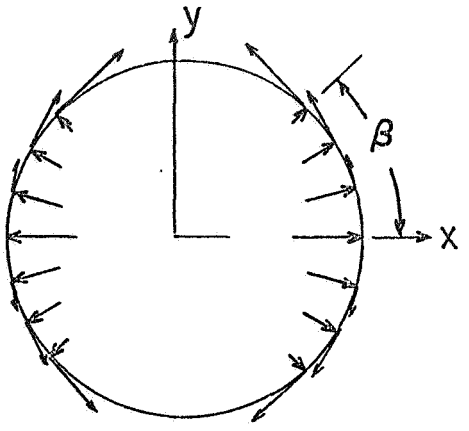

Boundary Condition at r = a

$$\sigma_r = \begin{cases} p\cos 2\theta & -\beta < \theta < \beta \\ 0 & \beta < \theta < \pi - \beta \end{cases}$$

$$\tau_{r\theta} = \begin{cases} -p\sin 2\theta & \pi - \beta < \theta < \pi + \beta \\ 0 & \pi + \beta < \theta < 2\pi - \beta \end{cases}$$

1-A-20

With boundary conditions (5) and (7) where An is defined by (6), the Fourier series representation of boundary conditions:

$$\sigma_r - i\,\tau_{r\theta} = \begin{cases} p(\cos 2\theta + i\sin 2\theta) = p\,e^{2i\theta}, & -\beta < \theta < \beta, \quad \pi - \beta < \theta < \pi + \beta \\ 0, & \beta < \theta < \pi - \beta, \quad \pi + \beta < \theta < 2\pi - \beta \end{cases}$$

1-A-21

Using (9) and computing for a_n and b_n:

$$\phi'(z) = \sum_{n=0}^{\infty} a_n z^{-n} = \frac{2p\beta}{\pi} a^2 z^{-2} + \sum_{m=2}^{\infty} \frac{p a^{2m}}{\pi(m-1)} \sin 2(m-1)\beta z^{-2m} \qquad \text{1-A-22}$$

$$\chi''(z) = \sum_{n=0}^{\infty} b_n z^{-n} = -\frac{p a^2}{\pi} \sin 2\beta z^{-2} - \frac{p a^4}{2\pi} \sin 4\beta z^{-4} + \frac{6p\beta}{\pi} a^4 z^{-4}$$

$$+ \sum_{m=2}^{\infty} \frac{(2m+1)}{\pi(m-1)} p a^{2(m+1)} \sin 2(m-1)\beta z^{-2(m+1)}$$

$$- \sum_{m=2}^{\infty} \frac{p a^{2(m+1)}}{\pi(m+1)} \sin 2(m+1)\beta z^{-2(m+1)} \qquad \text{1-A-23}$$

Calculation of Displacements:

Using (12) at $\rho = 1$

$$2G u_r \frac{\pi}{p a} = -2\xi\beta \cos 2\theta - \sum_{m=1}^{\infty} \frac{1}{m} \left[\frac{\xi}{2m+1} \cos 2(m+1)\theta \right.$$

$$\left. + \frac{1}{2m-1} \cos 2(m-1)\theta \right] \sin 2m\beta \qquad \text{1-A-24}$$

Calculation of Stresses:

Using (15) and (16)

$$\sigma_\theta \frac{\pi}{p} = 6\beta\rho^4 \cos 2\theta - \sum_{m=2}^{\infty} \frac{2\rho^{2m}}{m-1} \left[2m - 2 - (2m+1)\rho^2 \right] \sin 2(m-1)\beta \cos 2m\theta$$

$$- \sum_{m=0}^{\infty} \frac{\rho^{2(m+1)}}{m+1} \sin 2(m+1)\beta \cos 2m\theta \qquad \text{1-A-25}$$

$$\sigma_r \frac{\pi}{p} = 8 \beta \rho^2 \cos 2\theta + \sum_{m=2}^{\infty} \frac{\rho^{2m}}{(m-1)} [2 + 2m - (2m+1) \rho^2] \sin 2(m-1)\beta \cos 2m\theta$$

$$+ \sum_{m=0}^{\infty} \frac{\rho^{2(m+1)}}{(m+1)} \sin 2(m+1) \beta \cos 2m\theta \qquad \text{1-A-26}$$

$$\tau_{r\theta} \frac{\pi}{p} = 2 \beta \rho^2 (2 - 3\rho^2) \sin 2\theta$$

$$+ \sum_{m=2}^{\infty} \frac{\rho^{2m}}{(m-1)} [2m - (2m+1) \rho^2] \sin 2(m-1) \beta \sin 2m\theta$$

$$+ \sum_{m=0}^{\infty} \frac{\rho^{2(m+1)}}{(m+1)} \sin 2(m+1) \beta \sin 2m\theta \qquad \text{1-A-27}$$

C. NET RESULTS -- Obtained by Summing Solutions of A and B.

Net Radial Displacement

Add (14) and (24) to obtain the net radial displacement relation:

$$2 G u_r \frac{\pi}{p a} = -2\beta(1 + \xi \cos 2\theta) - \sum_{m=1}^{\infty} \frac{1}{m} \sin 2m\beta \left[\frac{\xi}{2m+1} \cos 2(m+1)\theta + \left(\frac{\xi}{2m-1} + \frac{1}{2m+1}\right) \cos 2m\theta + \frac{1}{2m-1} \cos 2(m-1)\theta \right] \quad \text{1-A-28}$$

At $\theta = 0$, radial displacements is maximum.

$$2 G u_{rmax} \frac{\pi}{p a} = -2\beta(1 + \xi) - \sum_{m=1}^{\infty} \frac{4(\xi + 1)}{(2m+1)(2m-1)} \sin 2m\beta \quad \text{1-A-29}$$

For the application of the results to the calculation of modulus of deformability, it is necessary to obtain a relation containing the integrated value of displacement.

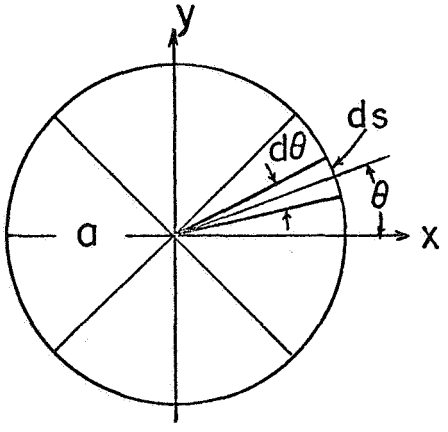

$$dy = ds \cos\theta = a \cos\theta \, d\theta$$

$$\left[2 G \bar{u}_r \frac{\pi}{p a}\right] a \sin\beta = \int_0^{\beta} [\text{R.H.S. (28)}] \, a \cos\theta \, d\theta \quad \text{1-A-30}$$

Replacing $\xi = 3 - 4\nu$ in the result gives:

$$\left[2 G \bar{u}_r \frac{\pi}{p a} \right] \sin\beta = -2\beta \left[\frac{5 - 4\nu}{2} \sin\beta + \frac{3 - 4\nu}{6} \sin 3\beta \right]$$

$$- \sum_{m=1}^{\infty} \frac{1}{2m} \sin 2m\beta \left[\frac{3 - 4\nu}{2m + 1} \left[\frac{\sin (2m + 1)\beta}{2m + 1} + \frac{\sin (2m + 3)\beta}{2m + 3} \right] \right.$$

$$+ \left[\frac{3 - 4\nu}{2m - 1} + \frac{1}{2m + 1} \right] \left[\frac{\sin (2m - 1)\beta}{2m - 1} + \frac{\sin (2m + 1)\beta}{2m + 1} \right]$$

$$\left. + \frac{1}{2m - 1} \left[\frac{\sin (2m - 3)\beta}{2m - 3} + \frac{\sin (2m - 1)\beta}{2m - 1} \right] \right] \qquad 1\text{-A-31}$$

Net σ_θ

Add (17) and (25) and rearrange the terms.

$$\sigma_\theta \frac{\pi}{p} = -2\beta\rho^2 + 6\beta\rho^4 \cos 2\theta + \sum_{m=0}^{\infty} \frac{\rho^{2(m+1)}}{m + 1} \sin 2(m + 1)\beta$$

$$\left[\cos 2m\theta + \left[(m + 1)\rho^2 - m \right] \cos 2(m + 1)\theta \right.$$

$$\left. + \left[(2m + 3)\rho^2 - 2m - 2 \right] \cos 2(m + 2)\theta \right] \qquad 1\text{-A-32}$$

At $\theta = \pi/2$, $\rho = 1$ σ_θ is maximum. Replacing

$$\cos 2m\theta = \begin{cases} +1 & m = 0, 2, 4, \ldots \\ -1 & m = 1, 3, 5, \ldots \end{cases}$$

into (32)

$$\sigma_\theta \, \pi/p = -8\beta \qquad 1\text{-A-33}$$

For $\beta = \pi/4$ $(Q = 2\ p)$:

$$\sigma_\theta = -Q \qquad \text{1-A-34}$$

This result checks with finite element analysis.

Net σ_r

Add (18) and (26) and rearrange the terms.

$$\sigma_r \frac{\pi}{p} = 2\beta\rho^2 \left[1 + (4 - 3\rho^2)\cos 2\theta\right] + \sum_{m=0}^{\infty} \frac{\rho^{2(m+1)}}{m+1} \sin 2(m+1)\beta$$

$$\left[\cos 2m\theta + \left[m + 2 - (m+1)\rho^2\right] \cos 2(m+1)\theta\right.$$

$$\left. + \left[2m + 4 - (2m+3)\rho^2\right] \cos 2(m+2)\theta\right] \qquad \text{1-A-35}$$

Net $\tau_{r\theta}$

Add (19) and (27) and rearrange the terms.

$$\tau_{r\theta} \frac{\pi}{p} = 2\beta\rho^2 (2 - 3\rho^2) \sin 2\theta + \sum_{m=0}^{\infty} \rho^{2(m+1)} \sin 2(m+1)\beta$$

$$\left[\frac{1}{m+1} \sin 2m\theta + 2(1 - \rho^2) \sin 2(m+1)\theta\right.$$

$$\left. + \frac{1}{m+1}\left[2m + 4 - (2m+5)\rho^2\right] \sin 2(m+2)\theta\right] \qquad \text{1-A-36}$$

Equation (31) is used in the calculation of the modulus of deformation in terms of applied pressures and corresponding deformations. Using Q = 2 p and d = 2 a, (31) can be rewritten as:

$$\left[\frac{2\,E\,\bar{u}_r}{2(1+\nu)}\,\frac{\pi}{p\,a}\right]\sin\beta = \text{R. H. S.}$$

$$E = \frac{(1+\nu)}{2\pi}\,\frac{Q\,d}{\bar{u}_d} = \frac{1}{\sin\beta}\,\frac{(1+\nu)\,d}{2\pi}\,\frac{Q}{\bar{u}_d}\left[\text{R. H. S.}\right]$$

$$E = K(\nu, \beta)\,\frac{Q\,d}{\bar{u}_d} \qquad \text{1-A-37}$$

Values of K (ν,β) are expressed in Table 2 for different values of ν and β. Q is the pressure actually applied to the rock (see 37). The variation of $K(\nu,\beta)$ with respect to β is shown in Figure 2 for values of ν = 0.25, 0.40, and 0.10. It is observed that K has a maximum value at $\beta = 45^{\circ}$, the case of the NX bore hole uniaxial jack.

CHAPTER 2

PERMEABILITY AND THERMAL CONDUCTIVITY STUDIES FOR LUNAR SURFACE PROBES

by

Paul A. Witherspoon and David F. Katz

CHAPTER 2

PERMEABILITY AND THERMAL CONDUCTIVITY STUDIES FOR LUNAR SURFACE PROBES

(Paul A. Witherspoon and David F. Katz)

I. INTRODUCTION

Among the objectives of man's study of the moon is an understanding of the flow of heat and fluids through lunar materials. This knowledge is not only of scientific value, but it is essential to the solution of engineering problems in exploring the moon. Two parameters of great importance are permeability and thermal conductivity.

From the scientific point of view, permeability is the dominant factor in hydraulic diffusivity. Thus, consideration of the emanation of vapors or liquids from the depths of the moon must depend upon a knowledge of the magnitude and variation of lunar permeability. In the analogous flow of heat, thermal conductivity is the controlling factor in thermal diffusivity. Thus, any studies of heat flow through the moon must take this parameter into account. Of course, permeability and thermal conductivity are rock properties of fundamental interest.

From the engineering standpoint, the many problems that man will face as he explores the moon will require a knowledge of both permeability and thermal conductivity of lunar materials. For example, the possibility exists of containing fluids in subsurface formations, either chambers or porous rocks, as suggested by current practice on earth. Low permeability formations may very well exist on the moon in which appropriate storage can be achieved, thereby eliminating the need for transporting containers from earth. In addition, the problem of fluid waste disposal may best be solved by using subsurface formations.

The extreme variation in temperature between lunar day and night will, in some cases, require the utilization of thermally insulating materials. Since rocks have an inherently low thermal conductivity, they may be very well-suited to this use. Hence, knowledge of the thermal conductivity of lunar rocks is essential.

In order that an adequate understanding of lunar permeability and thermal conductivity can be achieved, a representative series of measurements must be made. Clearly, the amount of lunar materials to be returned to earth for analysis will be inadequate. Thus, the feasibility of in situ measuring devices must be given serious consideration. Such devices should be easily transportable and capable of providing rapid measurements.

As a first approach to this problem, we propose that consideration be given to a surface probe, i.e., a device that will rest directly on the surface of the material to be measured. In determining permeability, a gas is injected into the material and appropriate pressure and flow rate measurements are made. In determining thermal conductivity, heat is transferred into the material and appropriate temperature and heat flow measurements are made. Details of these two devices will be discussed below.

In developing the theory for these devices, it was necessary to make certain simplifying assumptions. Specifically, the lunar material was assumed to be homogeneous and isotropic for both fluid and heat flow. The governing diffusion equations made use of zero initial pressure and temperature distributions throughout the material. While this is effectively true for fluid flow, it is of no mathematical consequence in either case, because the governing equations are linear and homogeneous.

In considering the feasibility of a surface probe, one must recognize that the lunar surface is composed of both consolidated and unconsolidated materials. In heat flow, the relative contribution of radiation to the overall heat transfer is strongly dependent upon the degree of consolidation. As porosity decreases, transfer by radiation also decreases, and conduction through the matrix becomes the dominant mode of heat flow. On the other hand, as porosity increases and the area of grain contacts diminishes, then radiation dominates the heat flow.

II. PERMEABILITY MEASUREMENT

A. Conceptual Description of Probe

A schematic drawing of the probe is given in Figure 2-1. The system basically consists of a holding chamber containing pressurized fluid, the disc source, and a pressure measuring device imbedded along with the source in a circular, impermeable skirt. The radius of the skirt is of the order of ten source radii.* The holding chamber contains the charge of gas for an individual measurement, and is connected by valves to the disc source and to a larger gas storage tank. A single switch releases the charge of gas, and activates a timer linked to the surface pressure tap. Constant source pressure is achieved by a servo connection between the release valve and an exit tap. The connecting valve between the holding chamber and the storage tank insures that only a small portion of the gas supply is consumed per measurement. This also allows for variation in source pressure as required by varying permeability. One can then compute permeability from a record of pressures and flow rates along with a knowledge of the rock porosity. Greater accuracy can probably be achieved by placement of additional pressure taps in the skirt, and suitable averaging of the individual measurements.

B. Unconsolidated Materials

In the earth's atmosphere, permeability of unconsolidated materials is usually determined utilizing the Kozeny-Carmen equation (Carman, 1956):

$$k = \frac{d_m^2 \phi^3}{180(1 - \phi)^2} \qquad (2\text{-}1)$$

where: k = permeability (cm^2)

d_m = the mean grain diameter (cm)

ϕ = porosity (dimensionless) defined as the ratio of the volume of the voids to the total bulk volume

---

*As can be seen from Figure 1-5, no sharp gradients exist beyond this region so that there is no effective flow out of the surface.

This equation was developed empirically for viscous laminar flow through a well-sorted mixture of spherical sand grains. As will be discussed below, flow of gases in the lunar environment may be rarified to the extent that viscous flow theory is inapplicable. Thus, calculations based on Equation 2-1 will yield, at most, only lower bounds to the effective permeabilities of lunar materials.

C. Consolidated Materials

1. Determination of flow regime. As discussed above, it is proposed that the surface probe utilize a gas for permeability measurement. Due to the high vacuum in the lunar environment, there exists a basic problem of determining the dominant flow regime.

As the average pore size and/or fluid pressure decrease, the fundamental nature of gas flow changes. The initial departure from viscous flow is the relaxation of the no slip boundary condition on the interstitial surfaces. The resulting, augmented flow, while still viscous in nature exhibits a greater temperature dependence than previously. As the effective degree of rarefaction increases further, the continuum nature of the fluid breaks down, and the flow must be modeled from a molecular point of view. In general, account must be taken of both intermolecular collisions, and collisions between molecules and the interstitial boundaries. However, when a high degree of rarefaction is achieved, the former become negligible due to the relative scarcity of fluid molecules. The fluid parameter indicative of the particular flow regime prevalent is the Knudsen number, defined here as $K_n \equiv \frac{\lambda}{d}$, where λ is the mean free path of the molecules of the fluid, and d an average pore dimension. For viscous flow, $K_n \ll 1$, whereas for the so-called Knudsen flow, $K_n \gg 1$.

To date, some analytic but virtually no experimental work has been done in attempting to model these various flow regimes in porous media. The most pertinent efforts are discussed below. However, the overall flow behavior in a surface probe system is a much more complex problem. In particular, the nature of the evolution of Knudsen flow, expected in the lunar surface, is difficult to foresee at this time. It seems likely that in the immediate neighborhood of the fluid source, the

flow will be viscous in nature, and, therefore, basically predictable by current techniques. However, the onset of Knudsen flow, and the possible effect this may have on the initial flow are difficult to surmise. At present, it is not certain how the overall flow of gases in lunar materials can be characterized.

It is also not certain what role adsorption will play as gases pass through lunar materials. This will not be a problem if steady state flow conditions prevail. For nonsteady flow, the significance of adsorption will depend largely upon the presence of residual gases deep in the lunar crust and the subsequent degree of outgassing at the surface.

The discussion that follows considers only viscous flow in detail. We will first analyze the isothermal flow of a slightly compressible fluid in porous media, this being the simplest case to treat mathematically. Next, we will examine the much more complex problem of compressible flow. Finally, we will consider briefly the flow of a rarefied gas.

2. Flow of viscous fluid in porous media. The dynamics of the viscous flow of a fluid in porous media are governed by the equation of conservation of mass

$$\phi \frac{\partial \rho}{\partial t} + \nabla \cdot (\rho \underline{v}) = 0 \tag{2-2}$$

and Darcy's law

$$\underline{v} = \frac{-k(p)}{\mu(p)} \nabla p \tag{2-3}$$

where: ϕ = porosity of the medium

ρ = density of the fluid (gm/cc)

t = time (sec)

$\underline{v}$ = the fluid velocity vector (cm/sec)

p = pressure in the fluid (dyne/cm^2)
k = permeability of the medium (cm^2)
μ = viscosity of the fluid (poise)

Combining Equations 2-2 and 2-3,

$$\nabla \cdot \left(\rho \frac{k(p)}{\mu(p)} \nabla p \right) = \phi \frac{\partial \rho}{\partial t} \tag{2-4}$$

For isothermal flow of a slightly compressible fluid, k and μ can be assumed constant, in addition, if spatial variation in ρ is neglected, we obtain the standard linear diffusion equation:

$$\nabla^2 p = \frac{\phi \mu c}{k} \frac{\partial p}{\partial t} \tag{2-5}$$

where c is the isothermal compressibility defined as

$$c \equiv \frac{1}{\rho} \frac{dp}{dp} \tag{2-6}$$

For isothermal flow of a compressible fluid, permeability can still be assumed constant, and we proceed from Equation 2-4 as follows. Utilizing the modified perfect gas law (Katz et al., 1959),

$$p = Z(p) \rho R T \tag{2-7}$$

where: $Z(p)$ = compressibility factor (dimensionless)
R = gas constant

Introduce now the integral transform (Al-Hussainy, Ramey, Crawford, 1966)

$$m(p) \equiv 2 \int_{p_0}^{p} \frac{p}{\mu(p)z(p)}\, dp \tag{2-9}$$

where p_0 is some reference pressure. Equation 2-8 then becomes:

$$\nabla^2 m(p) = \frac{\phi\mu(p)c(p)}{k} \frac{\partial m(p)}{\partial t} \tag{2-10}$$

Here we have made use of the relation:

$$c = \frac{1}{p} - \frac{1}{z(p)} \frac{dz(p)}{dp} \tag{2-11}$$

Equation 2-10 is, in general, nonlinear, as are Equations 2-8 and 2-9. However, it can be shown (Ruche, 1968) that for judicious choice of p_0, the reciprocal of diffusivity can be approximated by

$$\frac{\phi\mu(p)c(p)}{k} = bm^{\beta} \tag{2-12}$$

where b and β are constants. Thus, as the dependent variable, we can replace p by m; and our governing equation assumes the quasilinear form

$$\nabla^2 m = Dm^{\beta} \frac{\partial m}{\partial t} \tag{2-13}$$

where D is a constant.

A solution of Equation 2-13 corresponding to linear, one dimensional flow exists (Friedman, 1958); however, the axisymmetric problem for this equation corresponding to the disc source, has not yet been examined.

In the event that steady state conditions are reached, an approximate analogy between the flow of compressible and slightly compressible fluids is drawn as follows. Rearranging Equation 2-8, we have

$$\nabla^2 p^2 - \frac{d[\ln \mu(p)Z(p)]}{dp^2} (\nabla p^2)^2 = \frac{2\phi\mu(p)Z(p)}{k} \frac{\partial}{\partial t}\left(\frac{p}{Z(p)}\right)$$

$$= \frac{2\phi\mu(p)c(p)}{k} p \frac{\partial p}{\partial t} \qquad (2\text{-}14)$$

If it is assumed that viscosity and the compressibility factor are slowly varying functions of pressure, and/or that pressure gradients are small, the second term in Equation 2-14 can be neglected, and we obtain

$$\nabla^2 p^2 = \frac{\phi\mu(p)c(p)}{k} \frac{\partial p^2}{\partial t} \qquad (2\text{-}15)$$

It follows that steady flows of both slightly compressible and compressible fluids obey Laplace equations, in terms of pressure, and pressure squared, respectively.

3. Application of the disc source. Now consider the disc source utilizing a slightly compressible fluid. The flow is governed by

$$\frac{\partial^2 p}{\partial r^2} + \frac{1}{r}\frac{\partial p}{\partial r} + \frac{\partial^2 p}{\partial z^2} = \frac{\phi\mu c}{k} \frac{\partial p}{\partial t} \qquad (2\text{-}16)$$

$$p(r, z, 0) = 0 \qquad 0 \leq r < \infty, \; 0 \leq z < \infty \tag{2-17}$$

$$\frac{\partial p(r, 0, t)}{\partial z} = \frac{\mu}{k\pi a^2} Q \qquad t > 0, \; 0 \leq r < a \tag{2-18}$$

$$\frac{\partial p(r, 0, t)}{\partial z} = 0 \qquad t > 0, \; a < r < \infty \tag{2-19}$$

$$\lim_{r \to \infty} p(r, z, t) = 0 \qquad t > 0, \; 0 < z < \infty \tag{2-20}$$

Here, r and z are cylindrical polar coordinates (cm), a is the radius of the disc (cm), and Q the applied volumetric flow rate (cm^3/sec). The solution of this equation is fully documented by Selim, Fatt, and Somerton (1963). In general, permeability is determined numerically from the relation:

$$\frac{p(r, 0, t)\pi ka}{\mu Q} = H(1 - \tilde{r}) \left(\frac{\tau}{\pi}\right)^{1/2}$$

$$+ \frac{1}{\pi} \int_0^{\pi} \frac{1 - \tilde{r} \cos \theta}{(\tilde{r}^2 + 1 - 2 \tilde{r} \cos \theta)^{1/2}} \operatorname{erfc} \left[\frac{\tilde{r}^2 + 1 - 2 \tilde{r} \cos \theta}{\tau}\right]^{1/2} d\theta \tag{2-21}$$

$$- \frac{\tau^{1/2}}{\pi^{3/2}} \int_0^{\pi} \frac{1 - \tilde{r} \cos \theta}{1 + \tilde{r}^2 - 2 \tilde{r}^2 \cos \theta} \exp \left[- \frac{\tilde{r}^2 + 1 - 2 \tilde{r} \cos \theta}{\tau} \right] d\theta$$

where: $\tilde{r} \equiv \frac{r}{a}$ (dimensionless)

$\tau \equiv \frac{4kt}{a^2 \phi \mu c}$ (dimensionless)

erfc = the complementary error function

H = the Heaviside unit function defined:

$$H(x) = \begin{cases} 1 & x > 0 \\ 1/2 & x = 0 \\ 0 & x < 0 \end{cases} \tag{2-22}$$

Equation 2-21 is shown plotted in Figure 2-5. In the event that steady state is reached, Equation 2-21 simplifies to

$$\frac{p(r, 0)\pi ka}{\mu Q} = \frac{1}{\pi} \int_0^{\pi} \frac{1 - \tilde{r} \cos \theta}{(1 + \tilde{r}^2 - 2 \tilde{r} \cos \theta)^{1/2}} \, d\theta \tag{2-23}$$

This integral can be evaluated directly in terms of elliptic integral of the first and third kinds.

Here the approximate analogy between the flow of compressible and slightly compressible fluids, cf. Equation 2-15, is applicable, and the corresponding steady state solution for a compressible fluid becomes:

$$\frac{p^2(r, 0)\pi^2 k^2 a^2}{\mu^2 Q^2} = \frac{1}{\pi} \int_0^{\pi} \frac{1 - \tilde{r} \cos \theta}{(1 + \tilde{r}^2 - 2 \tilde{r} \cos \theta)^{1/2}} \, d\theta \tag{2-24}$$

Equations 2-23 and 2-24 are shown plotted in Figure 6.

4. Flow of a rarefied gas in porous media. A theory has been developed by Cercignani and Sernagiotto for the flow of a rarefied gas in a circular capillary (Cercignani, Sernagiotto, 1966). The analysis proceeds directly from the Boltzmann equation, and utilizes the Bhatnager-Gross-Krook model for the collision integral (see, Vincenti, Kruger, 1965). Diffuse reflection at the capillary wall is assumed, and a length-to-radius ratio large compared to 1 is required. The Boltzmann equation is subsequently reduced to an integral equation, which is solved numerically. As noted by the authors, the mass flow rate predicted is in excellent agreement

with experimental observation for all Knudsen numbers. Some particularly applicable work here is that of Lund and Berman (1966). While more general in scope than the above (finite length-to-radius ratio and some deviation from diffuse scattering at the wall), the analysis of this work is at best semi-empirical. The following expression is obtained for the dimensionless flow rate $\ddot{Q}$:

$$\hat{Q} = \frac{8F}{3[\sqrt{\pi} + (20/9B)\hat{\delta}]} + \frac{\hat{\delta}}{4}\left(1 + \frac{4.357}{1 + (0.592\sqrt{\pi}/B)\hat{\delta}}\right) \tag{2-25}$$

with

$$F = 1 + \frac{1.4327(\hat{\delta}/B)[0.8724(\hat{\delta}/B) - 1]}{1 + 19.429\ (\hat{\delta}/B) + 5.609\ (\hat{\delta}/B)^2 + 6.676\ (\hat{\delta}/B)^3} \tag{2-26}$$

Here, $\hat{Q}$ and $\hat{\delta}$ are, respectively, the dimensionless mass flow rate and inverse Knudsen number introduced by Cercignani and Sernagiotto (1966), while B is a collision integral parameter, of order one.

It should be emphasized that the above analyses are restricted to small relative pressure differences between ends of the capillary. The flow is then characterized by a constant Knudsen number, and is equally rarefied at all stations along the capillary. When the pressure difference between capillary ends is a significant fraction of the average pressure, some recent experimental data are available (Sreekanth, 1968). As a result, this case is more pertinent to the lunar problem. However, no rigorous theory appears to exist currently for this case.

Huang and Ramsey have suggested an interpolating formula for predicting flow through capillaries at arbitrary rarefaction and pressure variation, and have extended the analysis to porous media (Huang, Ramsey, 1968). For an ensemble of circular capillaries, they give

$$\frac{Q_0 L}{\bar{A}(\Delta p/p_0)} = C + E\,\frac{\Delta p}{p_0} \tag{2-27}$$

where

$$C = f\bar{D}_{KA}\left[0.7118 + 0.0736\left(\frac{2\bar{r}}{\lambda_0}\right)\left(\frac{p_2}{p_0}\right)\right] \tag{2-28}$$

$$E = f\bar{D}_{KA}\left[0.0368\left(\frac{2\bar{r}}{\lambda_0}\right)\right] \tag{2-29}$$

The subscripts 0, 1, 2 refer to reference conditions, and conditions at the front and back ends of the capillary, respectively. Here L is the length of the capillary; $\bar{r}$ the radius, representative of a mean pore radius; f a dimensionless constant, determined experimentally, relating the capillary arrangement to the total flow rate (i.e., the effective area fraction); $\bar{A} = \pi\bar{r}^2$; $\Delta p = (p_1 + p_2)/2$, and $\bar{D}_{KA}$ the Knudsen diffusivity; $\bar{D}_{KA} \equiv 2\bar{v}\bar{r}/3$, where $\bar{v}$ is the mean molecular speed. $\bar{v} = (8\,RT/\pi)^{3/2}$ where T is temperature. However, the validity of this interpolation scheme is not assured, and the experimental evidence is limited to the case of atmospheric pressure on the low pressure side.

5. Practical considerations. In the design of a surface permeability probe, due consideration must be given to size, weight, durability requirements, etc. Conceptually, it seems feasible to utilize a waste gas, such as CO_2. In view of current practice on earth, a miniaturization of the probe is suggested. However, any miniaturization is limited by the requirement that the source diameter be large compared to the pore dimensions.

The possibility of obtaining steady state measurements can be examined only in an approximate sense from the form of the dimensionless time for flow of a slightly compressible fluid, $\tau = 4\,kt/\phi\mu ca^2$. We let $\tau = 10^5$ correspond to steady state, and take $\phi = 0.2$, $\mu = 0.01$

centipoises, a = 1 mm, and consider an "average" pressure of 1 psi. For high permeability rocks, $k \simeq 10^{-8}$ cm^2, t is of the order of a few minutes, whereas for low permability rocks, $k \simeq 10^{-14}$ cm^2, t is of the order of years. Thus, steady state measurements would only appear possible for high permeabilities.

Surface devices geometrically similar to the one proposed here have been successfully used to determine the permeability of soils on earth. A fundamental description is presented by Evans and Kirkham (1949). Notably, the theory requires experimental determination of an effective shape factor, and is applicable only to steady state measurements.

In an attempt to gain merely some physical feeling for such a probe, some highly simplified preliminary experiments were conducted. A crude probe was used, consisting of a small diameter (1/4 in.) copper tubing inserted through a rubber stopper. The dimensions are much larger than for the envisioned lunar probe. The stopper was placed firmly against flat surfaces of selected rock samples, and air was pumped through the tube. Utilizing Darcy's law for spherically symmetric flow, permeabilities were calculated which were of the same order of magnitude as the values obtained from conventional means.

III. THERMAL CONDUCTIVITY MEASUREMENT

A. Measurement with Surface Contact Probe

1. Conceptual description of probe. In this section, two simple configurations are examined, one utilizing a disc source, the other a ring source, cf. Figures 2-2 and 2-3. In both configurations, the heat source and a contact temperature sensor are imbedded in an insulating circular skirt; the radius of the skirt is of the order of ten source radii.* For the ring source, the sensor is positioned at the center of the ring. For the disc source, the sensor can be positioned at an arbitrary station in the skirt and, as in the case of the disc fluid source, accuracy may be improved by use of additional sensors.

---

*Beyond this value of r, no sharp temperature gradients exist, and there is no effective heat flow out of the surface.

A single switch activates the heat source and a timer linked to the temperature sensor. A record of material surface temperature versus time is thus achieved. If a constant heat input is maintained, and the density and heat capacity of the material are known or assumed, thermal conductivity can then be calculated.

The analysis here assumes perfect thermal contact between heat source and lunar material. This is an idealization and is discussed below.

a. Disc heat source. The temperature distribution due to a disc heat source is analogous to the pressure distribution resulting from a disc source utilizing a slightly compressible fluid. We simply replace $\frac{\pi kap}{\mu Q}$ by $\frac{\kappa T}{aQ}$ and $\frac{k}{\phi\mu c}$ by α in Equation 2-21 and Figure 2-5.

$$\frac{\kappa T(\tilde{r},\ 0,\ \tau)}{aQ} = H(1-\tilde{r})\left(\frac{\tau}{\pi}\right)^{1/2} +$$

$$+\frac{1}{\pi}\int_0^{\pi}\frac{1-\tilde{r}\cos\theta}{(\tilde{r}^2+1-2\tilde{r}\cos\theta)^{1/2}}\operatorname{erfc}\left[\frac{\tilde{r}^2+1-2\tilde{r}\cos\theta}{\tau}\right]^{1/2}d\theta + \qquad (2\text{-}30)$$

$$-\frac{\tau^{1/2}}{\pi^{1/2}}\int_0^{\pi}\frac{1-\tilde{r}\cos\theta}{1+\tilde{r}^2-2\tilde{r}\cos\theta}\exp\left[-\frac{\tilde{r}^2+1-2\tilde{r}\cos\theta}{\tau}\right]d\theta$$

where: κ = thermal conductivity (cal/cm sec °K)

α = thermal diffusivity (cm^2/sec)

T = temperature (°K)

Q = the constant heat rate/unit area supplied (cal/cm^2 sec)

$\tau = 4\ \alpha t/a^2$ (dimensionless)

b. Ring heat source. The temperature distribution due to a ring source is governed by:

$$\frac{\partial^2 T}{\partial r^2}+\frac{1}{r}\frac{\partial T}{\partial r}+\frac{\partial^2 T}{\partial z^2}=\frac{1}{\alpha}\frac{\partial T}{\partial t} \qquad (2\text{-}31)$$

$$T(r, z, 0) = 0 \qquad 0 \leq r < \infty,\ 0 \leq z < \infty \tag{2-32}$$

$$\frac{\partial T}{\partial z}(r, 0, t) = 0 \qquad t > 0,\ 0 \leq r \neq a < \infty,\ 0 \leq z < \infty \tag{2-33}$$

$$\lim_{r \to \infty} T(r, z, t) = 0 \qquad t > 0,\ 0 \leq z < \infty \tag{2-34}$$

The effect of the ring source can be accounted for by distributing an instantaneous heat source of fixed strength uniformly about a circle of radius a in the plane z = 0, and then integrating to time t. If follows that the temperature measured by the sensor is:

$$T(0, 0, \tau) = \frac{q}{2\pi a} \operatorname{erfc} \frac{a}{\sqrt{4\alpha t}} \tag{2-35}$$

where q is the constant rate of heat input. A device of this type has been successfully applied to the laboratory measurement of rock conductivity (Mossahebi, 1966).

c. The problem of contact resistance. Whenever an interface between two contacting materials is not geometrically smooth, there exists an effective resistance to heat flow across the interface due to the nonuniformity of the thermal contact. Clearly such contact resistance will exist for any surface thermal probe. Few attempts have been made at analyzing this general problem and one is not attempted here. However, it does seem physically reasonable that the magnitude of the contact resistance will increase as:

(1) the height of any surface protrusions increases

(2) the net contact area between the surfaces decreases

(3) the thermal conductivities of the two surfaces increase

These postulates are confirmed in an analysis by Fenech and Rohsenow (1963). They derive an expression for the effective conductance, in the absence of radiation, of a nonuniform interface idealized to consist of cylindrical protrusions. Applied to our disc probe, this becomes:

$$h_c = \frac{4.26\sqrt{n}}{(1-\varepsilon^2)(1/\kappa_p) + (4.26\sqrt{n}\,\delta/\varepsilon)/\kappa} \tag{2-36}$$

where: h_c = the interface conductance (cal/cm sec °K, $h_c = \infty$ for perfect thermal contact)

κ_p = thermal conductivity of the probe (cal/cm sec °K)

κ = thermal conductivity of lunar material (cal/cm sec °K)

δ = the height of an average lunar surface protrusion (cm, assuming the disc is smooth)

n = the average number of protrusions contacting the disc per unit area

ε = A_c/A, A_c being the contacting area of an average protrusion and $A = \pi a^2$, the surface area of the disc

Notably, for $\kappa_p \ll \kappa$, the effect of the nonuniform contact is diminished. Hence, a design criterion for the disc heat source is that its thermal conductivity be small compared to that of the lunar material.

d. Significance of radiative transfer. In the preceding analysis, thermal conductivity has been assumed constant, independent of temperature. Subsequently, the influence of radiative heat transport has been neglected. For particulate materials and vesicular materials of high porosity, the relative contribution of radiation to heat transport may be quite significant in the lunar temperature range. In the event that lunar material is used in constructing a heat shield, a knowledge of the significance of radiation would be necessary. In general, whenever

sharp temperature gradients exist, radiative heat transfer and the temperature dependence of the material conductivity will probably be important. Some basic studies have been made in this area (Wechsler and Glaser, 1964; Linsky, 1966; Halajian et al., 1967; Ulrichs, 1968), but there is a clear-cut need for additional work with appropriate experimentation, particularly for consolidated materials.

2. Practical considerations. In the design of any portable device for in situ measurement, due consideration must be given to size, weight, durability, power requirements, etc. Conceptually, the surface contact probe presents no difficulties in this respect. However, any miniaturization is limited by the requirement that the source diameter be large compared to the dimension of any surface cracks or protrusions. Present knowledge of the lunar surface would seem to indicate that a source diameter of the order of one centimeter is feasible. The possibility of obtaining steady state measurements can be examined directly from the form of the dimensionless time in Equation 2-30, $\tau = 4\ \alpha t/a^2$. Letting $\tau = 10^5$ correspond to steady state, cf. Figure 2-5, and considering the maximum expected value of thermal diffusivity, $\alpha = 10^{-3}$ cm^2/sec, we have

$$\frac{t}{a^2} = 2.5 \times 10^7 \text{ sec/cm}^2$$

For a source diameter of one centimeter, steady state would be achieved at the earliest after approximately eight weeks, and thus such measurements do not appear feasible.

In the surface thermal probe, a contact temperature sensor is imbedded in an insulating skirt which rests on the lunar material. A requirement for the sensor is therefore that it be essentially nonconducting and/or of such small size that the insulating nature of the surface boundary be preserved. Since the measurements will be transient, the sensor must have a fast response time. In addition, there are the usual requirements of accuracy, sensitivity, and stability.

In view of these general requirements and the desirability of a simple data readout, the platinum resistance thermometer and quartz crystal transducer seem to be the most suitable of the currently marketed devices. In addition, a fairly recent device still under development, the nuclear quadrupole resonance thermometer (NQR), should be given serious consideration. The NQR thermometer has the following basic advantages: (1) digital output, (2) long-term stability, (3) high sensitivity, (4) direct measurement of absolute temperature, (5) solid state design, and (6) low voltage requirements (Lunar Heat Flow Measurement, 1966).

B. Possible Use of Remote Sensing Probe

A problem inherent in any contact surface probe design is the non-uniformity of thermal contact due to surface roughness of the material being measured. In general, the significance of contact resistance is difficult to analyze. Therefore it seemed reasonable to examine, if in but a highly simple-minded manner, the feasibility of a device in which neither the neat source nor temperature sensor were in contact with the lunar material.

The idea of a remote sensing thermal probe is not a new one, and was incorporated in two earlier design studies for multipurpose borehole probes (Lunar Surface and Subsurface Probes for Apollo Application Program, 1966; Study of Lunar Geophysical Surface and Subsurface Probes for Apollo Application Program, 1966). The concept introduced here, while different in layout employs the same electronics as in these earlier schemes. That is, it is proposed that surface temperature be measured by an infrared device of the Michaelson interferometer type making use of a bolometer detector. Surface spectral emissivity is measured by an infrared spectrometer.

A schematic of the system is contained in Figure 4. The surface is heated by a symmetric element such as a ring source. In the center of the source is the electronics package, which is thermally insulated from the source. Further insurance that source emission does not influence temperature measurement could be provided by making such measurements after the source has been activated for a given time.

An additional, outer shield protects the surface from any solar radiation. Just as for the proposed surface contact probes, a record of surface temperature versus time, along with the heat input and a knowledge of density and heat capacity, would yield thermal conductivity.

IV. CONCLUSIONS

In summary, this report has presented some basic analysis of fluid flow through porous media, and simplified approaches to the problem of in situ measurement of lunar permeability and thermal conductivity. It is our conclusion, that there is a definite need for the following investigations:

A. Theoretical and experimental work on fluid flow through consolidated materials in vacuo.

B. Experimental work on applicability of surface probes in measuring permeability of soils and rocks in vacuo.

C. Basic experimental work on heat flow through both consolidated and unconsolidated materials in vacuo.

D. Experimental work on applicability of surface probe for in-vacuo measurement of thermal conductivity.

REFERENCES

1. Al-Hussainy, R., Ramey, H. J., and Crawford, P. B. (1966), "The Flow of Real Gases through Porous Media," Jour. Pet. Tech., V. 18, No. 6, p. 624, 1966.

2. Carman, P. C. (1956), Flow of Gases Through Porous Media, Academic Press, New York, p. 11ff.

3. Cercignani, C., and Sernagiotto, F. (1966), "Cylindrical Poiseuille Flow of a Rarefied Gas," Phys. Fluids, V. 9, No. 1, p. 40.

4. Evans, D. D., and Kirkham, D. (1949), "Measurement of the Air Permeability of Soil in Situ," Soil. Sci. Soc. Amer. Proc., V. 13, p. 65.

5. Fenech, H., and Rohsenow, W. M. (1963), "Prediction of Thermal Conductance of Metallic Surfaces in Contact," ASME Jour. Heat Transfer, V. 85, p. 15.

6. Friedmann, N. E. (1958), "Quasilinear Heat Flow," Transactions of the ASME, V. 80, p. 635.

7. Halajian, J. D., Reichman, J., and Karafiath, L. L. (1967), "Correlation of Mechanical and Thermal Properties of Extraterrestrial Materials," Grumman Aircraft Engineering Corp., Research Department, Report No. RE-280, Jan.

8. Huang, T. H., and Ramsey, T. L. (1968), "Fluid Flow in Porous Media — Diffusion and Flow of Nitrogen Gas in Natural Rocks," paper presented at A.G.U. annual meeting, April 1968.

9. Katz, D. L., et al. (1959), Handbook of Natural Gas Engineering, McGraw Hill, New York, P. 96.

10. Linsky, J. L. (1966), "Models of the Lunar Surface Including Temperature-Dependent Thermal Properties," Harvard College Observatory, Scientific Report No. 8, NASA Research Grant No. NGS 64-60, Jan.

11. "Lunar Heat Flow Measurement (1966)," Corporate IR&D Study, Systems Division, The Bendix Corporation, Project No. 4577, Final Report, Sept.

12. "Lunar Surface and Subsurface Probes for Apollo Application Program (1966)," Texaco Experiment, Inc., Final REport TP-277, NASA Contract No. NAS 8-20085, May.

13. Lund, A. M., and Berman, A. S. (1966), "Flow and Self Diffusion of Gases in Capillaries, I and II," Jour. Appl. Phys., V. 37, pp. 2489 and 2496.

14. Mossahebi, M. (1966), "Thermal Conductivity of Rocks by a Ring Source Device," M. S. Thesis, Univ. of Calif., Berkeley, 1966.

15. Ruche, M. (1968), Department of Civil Engineering, Univ. of Calif., Berkeley, private communication.

16. See, e.g., Vincenti, W., and Kruger, C. (1965), Introduction to Physical Gas Dynamics, McGraw Hill, New York, P. 376, 1965.

17. Selim, M. A., Fatt, I., and Somerton, W. H. (1963), "Temperature Rise in a Semi-Infinite Medium Heated by a Disc Source," Koninkl. Nederl Akademie Van Metenschappen-Amsterdam, Proceedings, Series A, V. 66, No. 5 and Indag. Math., V. 25, No. 5.

18. Sreekanth, A. (1968), paper to be presented at 6th Symposium on Rarefied Gas Dynamics, July 1968.

19. "Study of Lunar Geophysical Surface and Subsurface Probes for Apollo Application Program (1968)," Electro-Mechanical Res., Inc., NASA Contract No. NAS 8-20243, June.

20. Ulrichs, J. (1968), research currently being conducted at the center for radiophysics and Space Research, Cornell Univ., Ithaca, N. Y., private communication.

21. Wechsler, A. E., and Glaser, P. E. (1964), "Thermal Conductivity of Non-Metallic Materials," Arthur D. Little, Inc., Summary Report, NASA Contract No. NAS 8-1567.

SYMBOLS

a radius of fluid (or heat) source

$A \equiv \pi a^2$ area of disc source

$\overline{A} \equiv \pi \overline{r}^2$ cross sectional area of an average pore

A_c contacting area of average protrusion

b constant [cf. Equation 2-12]

B dimensionless collision integral parameter

c isothermal compressibility

C constant [cf. Equation 2-28]

d average pore dimension

d_m median grain diameter

D constant [cf. Equation 2-13]

$\overline{D}_{KA} \equiv 2\,\overline{v}\,\overline{r}/3$ Knudsen diffusivity

E reference constant [cf. Equation 2-29]

f effective area fraction

F function of $\hat{\delta}$ and B [cf. Equation 2-26]

h_c interface conductance

H Heaviside unit function

k permeability

Kn Knudsen number

m integral transform of pressure [cf. Equation 209]

n number of protrusions/unit area contracting disc source

p pressure

p_0 reference pressure

p_1 pressure at front of capillary

p_2 pressure at end of capillary

q heat flow rate

Q dimensional volumetric flow rate

Q_0 dimensional volumetric flow rate

$\hat{Q}$ dimensionless mass flow rate

r radial coordinate in cylindrical polar system

$\bar{r}$ capillary radius

$\tilde{r}$ $\equiv$ r/a dimensionless radial coordinate in cylindrical polar system

R gas constant (for a particular gas)

t time

T temperature

v velocity

$\bar{v}$ mean thermal speed

x dummy variable

z axial coordinate in cylindrical polar system

Z compressibility

α thermal diffusivity

β constant [cf. Equation 2-12]

δ average height of surface protrusion

$\hat{\delta}$ inverse Knudsen number

ε $\equiv$ Ac/A

θ dummy variable

κ thermal conductivity of porous medium

κ_p thermal conductivity of probe

λ mean free path

λ_0 mean free path at reference conditions

μ viscosity

ρ density

τ $\equiv 4\ kt/a^2\phi\mu c$ dimensionless time

ϕ porosity

Q applied heat flow rate/unit area

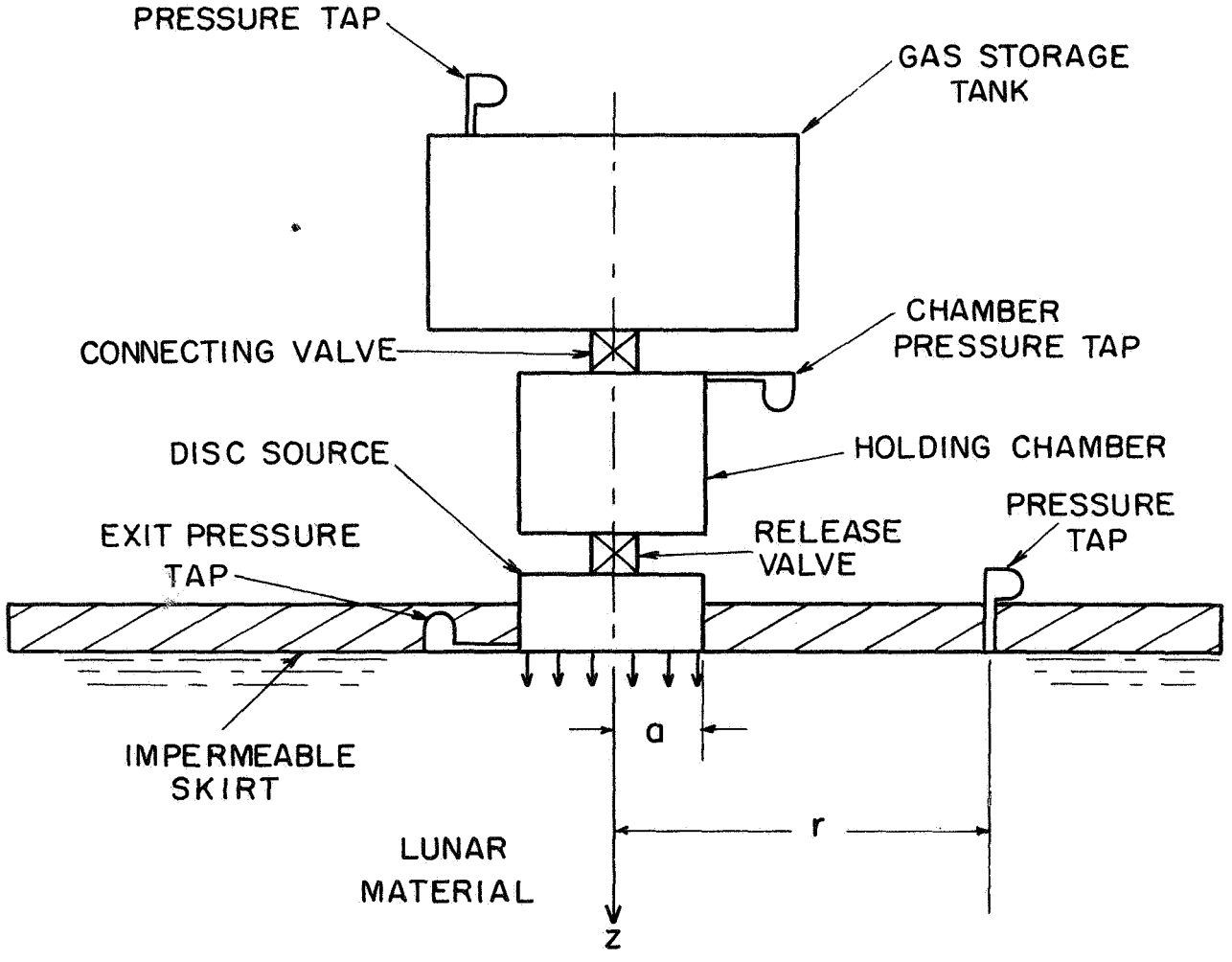

PERMEABILITY PROBE.

FIG 2-1

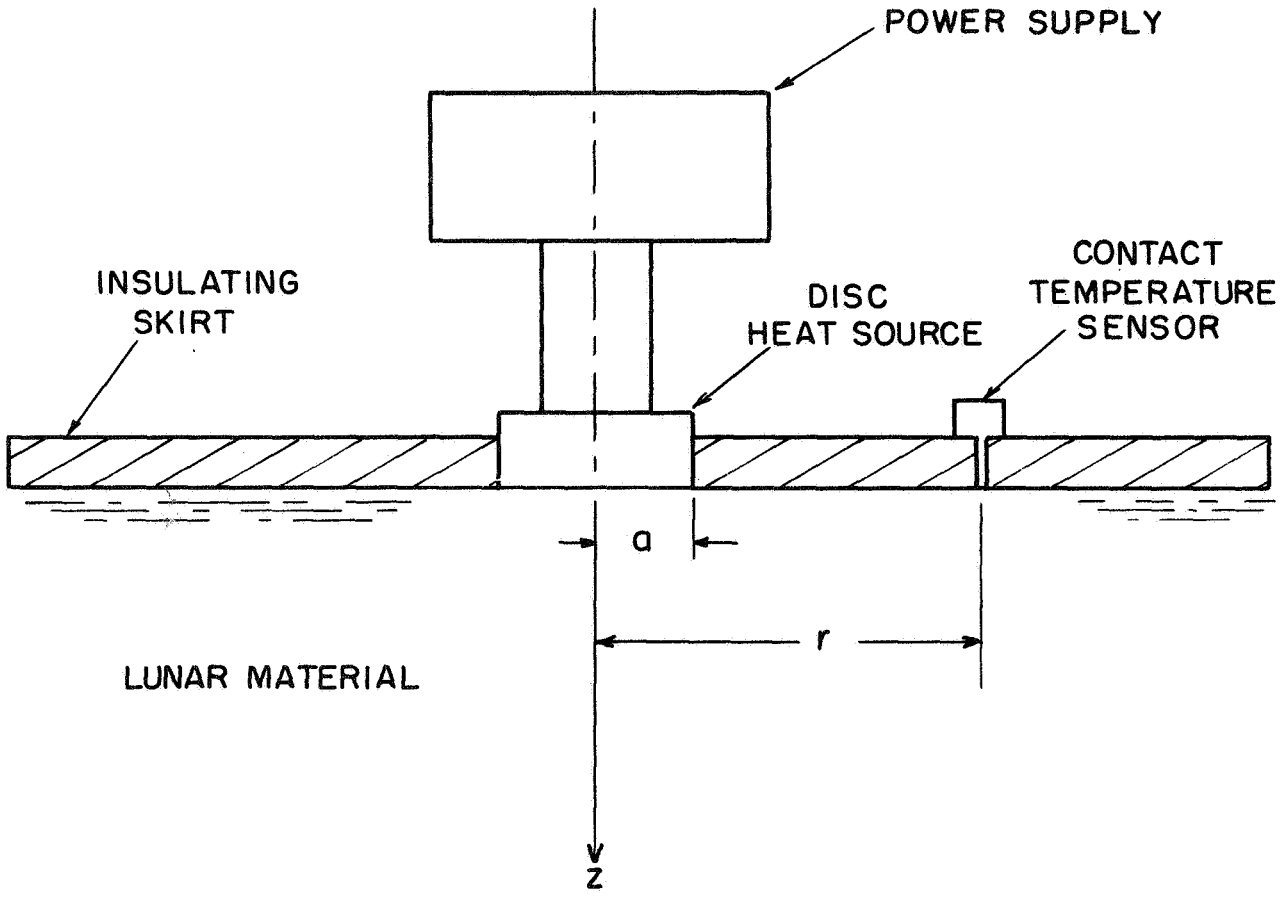

DISC SOURCE THERMAL PROBE.

FIG 2-2

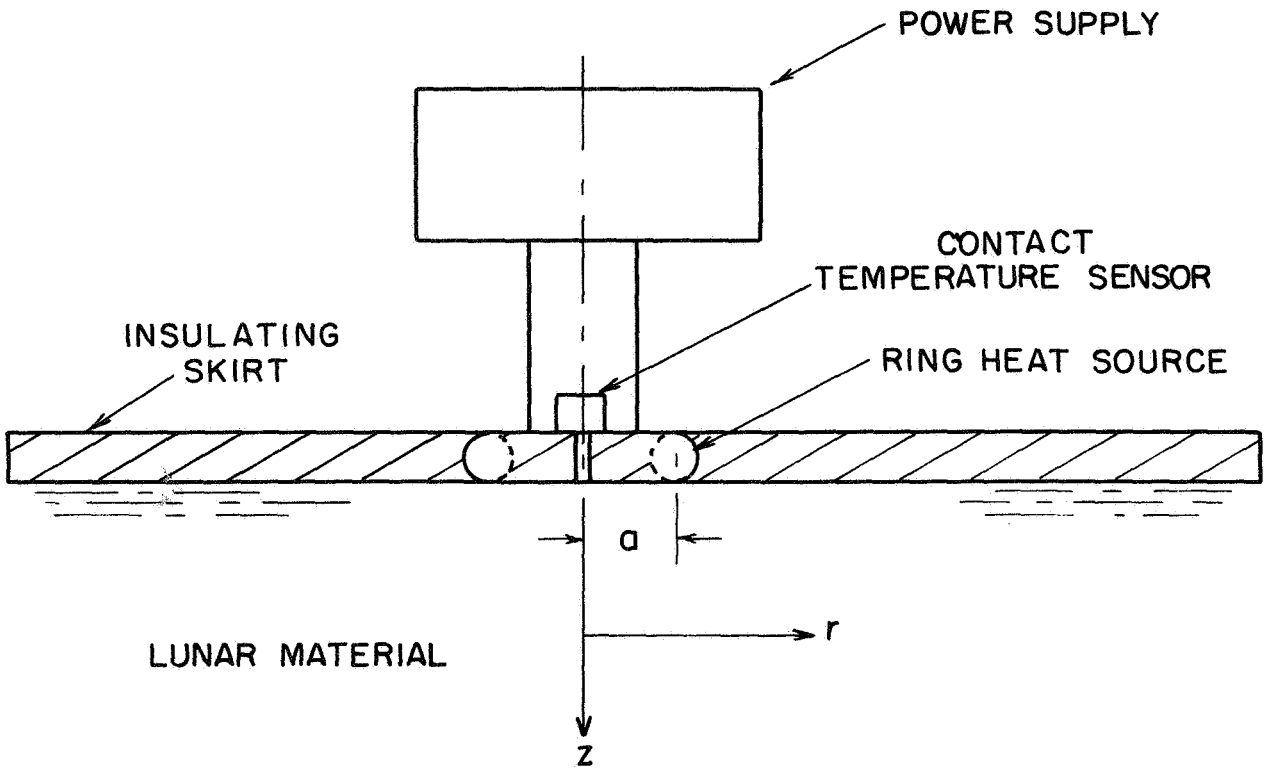

RING SOURCE THERMAL PROBE.

FIG 2-3

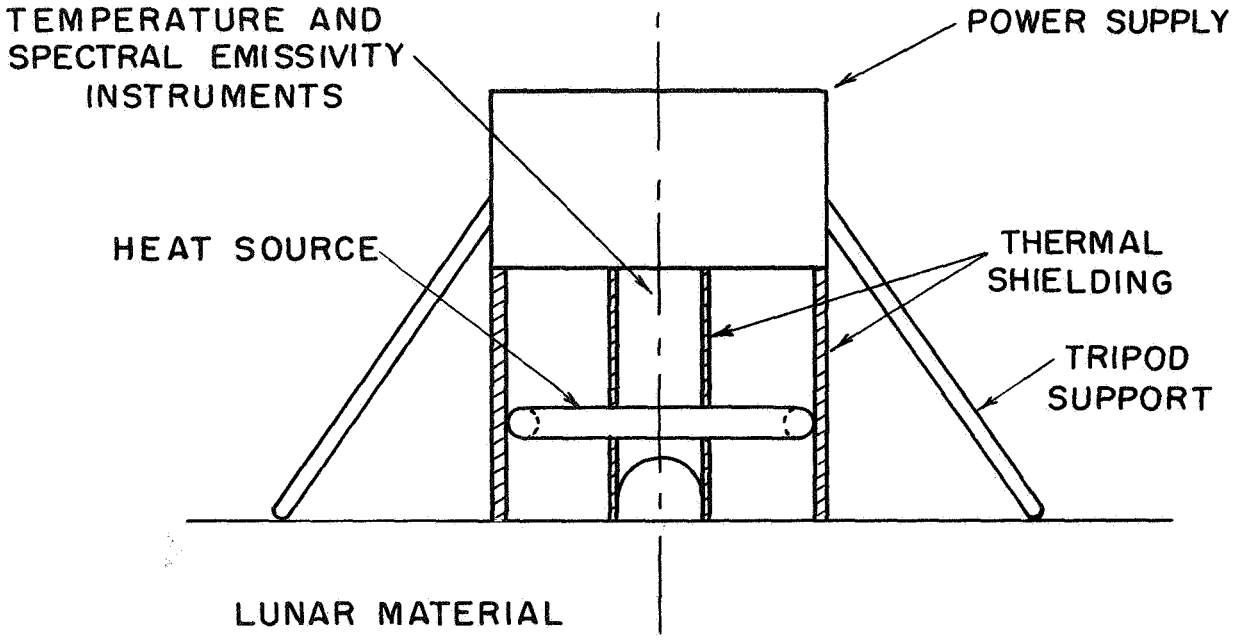

SURFACE REMOTE SENSING THERMAL PROBE.

FIG 2-4

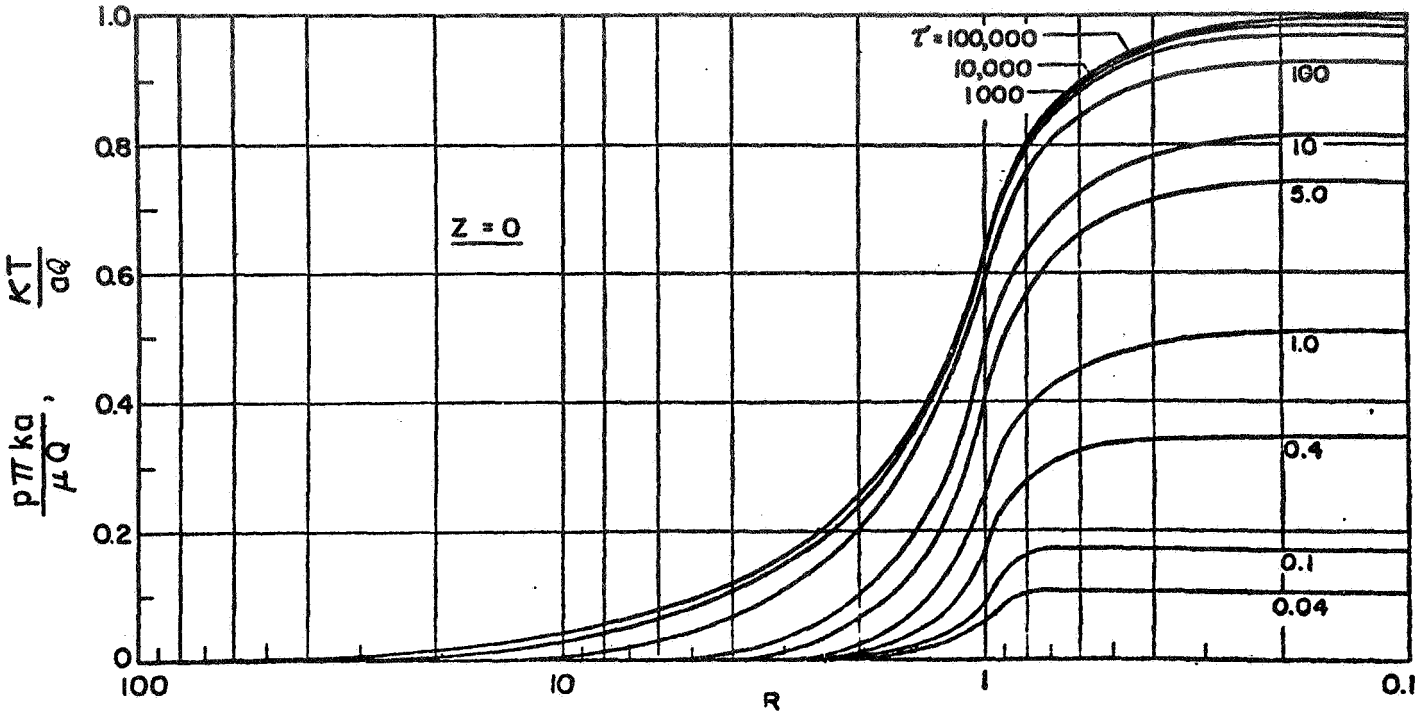

FIG 2-5: Dimensionless pressure and temperature rise at the surface for disc source (after Selim, Fatt, and Somerton [17]).

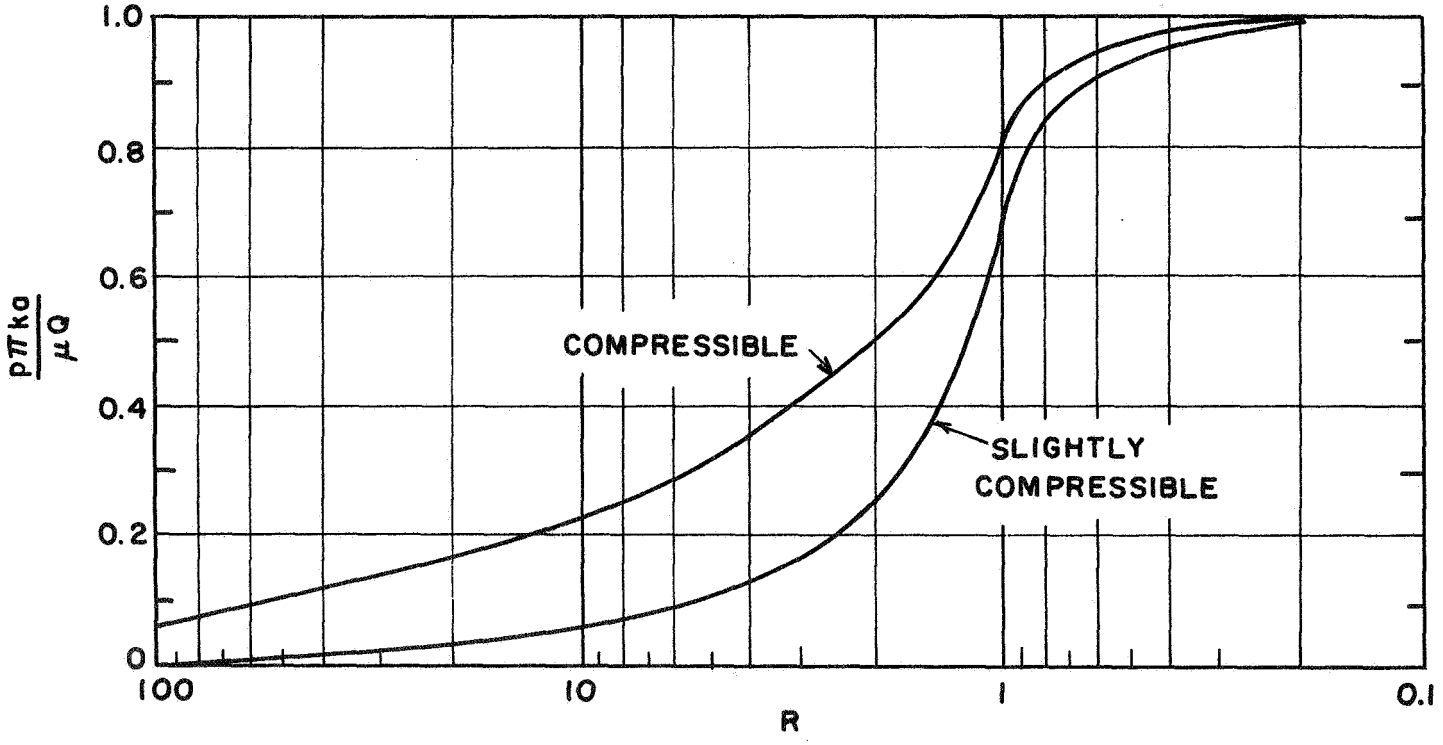

FIG 2-6: Steady state dimensionless pressure at the surface for disc source with compressible and slightly compressible fluids.